

İSTANBUL TECHNICAL UNIVERSITY ★ INSTITUTE OF SCIENCE AND TECHNOLOGY

**STEADY-STATE AEROELASTIC ANALYSIS AND NUMERICAL DESIGN
OPTIMIZATION OF AIRCRAFT STRUCTURES**

**M.Sc. Thesis by
Arda YANANGÖNÜL**

Department : Aeronautics and Astronautics

Programme : Aeronautics and Astronautics

JUNE 2009

**STEADY-STATE AEROELASTIC ANALYSIS AND NUMERICAL DESIGN
OPTIMIZATION OF AIRCRAFT STRUCTURES**

**M.Sc. Thesis by
Arda YANANGÖNÜL
(511061003)**

**Date of submission : 04 MAY 2009
Date of defence examination: 09 JUNE 2009**

**Supervisor (Chairman) : Assist. Prof. Dr. Melike NİKBAY (İTÜ)
Members of the Examining Committee : Prof. Dr. Zahit MECİTOĞLU (İTÜ)
Prof. Dr. Ata MUĞAN (İTÜ)**

JUNE 2009

İSTANBUL TEKNİK ÜNİVERSİTESİ ★ FEN BİLİMLERİ ENSTİTÜSÜ

**UÇAK YAPILARININ DAİMİ REJİMDE AEROELASTİK ANALİZİ VE
SAYISAL TASARIM OPTİMİZASYONU**

**YÜKSEK LİSANS TEZİ
Arda YANANGÖNÜL
(511061003)**

**Tezin Enstitüye Verildiği Tarih : 04 Mayıs 2009
Tezin Savunulduğu Tarih : 09 Haziran 2009**

**Tez Danışmanı : Yrd. Doç. Dr. Melike NİKBAY (İTÜ)
Diğer Jüri Üyeleri : Prof. Dr. Zahit MECİTOĞLU (İTÜ)
Prof. Dr. Ata MUĞAN (İTÜ)**

HAZİRAN 2009

FOREWORD

I would like thank my thesis advisor Assist. Prof. Dr. Melike NIKBAY for providing her support and knowledge through this work. I would like to express my appreciation for TÜBİTAK who supported me through project “Analysis and Reliability Based Design Optimization of Fluid-Structure Interaction Problems Subject To Instability Criteria” with grant number 105M235. I acknowledge Prof. Kurt MAUTE’s and Michel LESOINNE’s support and valuable suggestions. Lastly, I also thank Levent ÖNCÜ and Ahmet AYSAN for their constant help.

June 2009

Arda YANANGÖNÜL
Aeronautical Engineer

TABLE OF CONTENTS

	<u>Page</u>
ABBREVIATIONS	viii
LIST OF TABLES	ix
LIST OF FIGURES	xi
SUMMARY	xiii
ÖZET	xv
1. INTRODUCTION	1
1.1 Purpose and Outline of the Thesis	1
2. REVIEW OF AEROELASTICITY AND MDO	3
2.1 Review of Aeroelasticity	3
2.2 Review of MDO	12
3. NUMERICAL DESIGN OPTIMIZATION	15
3.1 Application of Numerical Design Optimization	15
3.2 Problem Formulation	16
3.3 Structural Analysis Model	16
3.4 Optimization Variables	17
3.5 Optimization Methodology	20
3.6 Optimization Results	22
3.7 Conclusion	25
4. AEROELASTIC ANALYSIS	27
4.1 Introduction	27
4.2 Aeroelastic Solver AERO-F-S	27
4.3 Implementation of Finite Element Model with Orthotropic Properties	33
4.4 Model Validation	37
4.4.1 Structural Model Validation	38
4.4.2 Aerodynamic Model Validation	39
4.5 Steady-state Aeroelastic Analysis	40
4.6 Conclusion	41
5. CONCLUSION AND FUTURE WORK	43
REFERENCES	44
APPENDICES	49
CURRICULUM VITAE	59

ABBREVIATIONS

ALE	: Arbitrary Lagrangian Eulerian
CAA	: Computational Aeroelasticity
CFD	: Computational Fluid Dynamics
CSD	: Computational Structural Dynamics
FEA	: Finite Element Analysis
FEM	: Finite Element Method
MDO	: Multidisciplinary Optimization

LIST OF TABLES

	<u>Page</u>
Table 2.1: Methodology Comparison in CAA.....	11
Table 3.1: Structural analysis results of the reference wing	17
Table 3.2: Pareto set for the problem	23
Table 4.1: Comparison of calculated frequencies with experimental data	39
Table 4.2: Displacement comparison at leading and trailing edges.....	41

LIST OF FIGURES

	<u>Page</u>
Figure 3.1 : Pareto optimal solution graph.....	24
Figure 3.2 : Thickness variation of structural elements along the span.....	25
Figure 4.1 : Staggered algorithm for computation of the aeroelastic steady-state....	31
Figure 4.2 : 8 noded hexahedral element	34
Figure 4.3 : AGARD 445.6 wing geometry.....	38
Figure 4.4 : Constitutive matrix corresponding to orthotropic matrix.....	38
Figure 4.5 : Deflected and undeflected wing	40
Figure A.1 : The optimization variables and meshed model of wing structure	50
Figure A.2 : Quad dominated structural mesh of the wing.....	50
Figure A.3 : Displacement field of reference wing under static load (mm)	51
Figure A.4 : Stress field of reference wing under static load (MPa)	51
Figure A.5 : Optimization logical flowchart.....	52
Figure B.1 : Computed modal shapes compared to experimental data.....	53
Figure B.2 : Coarse CFD grid with 403321 tetras	54
Figure B.3 : Close-up to the wet surface of the wing	54
Figure B.4 : Pressure contours for the upper surface of rigid wing, present study....	55
Figure B.5 : Pressure contours for the upper surface of the rigid wing, Liu [11].....	55
Figure B.6 : Pressure contours for the lower surface of rigid wing, present study....	56
Figure B.7 : Pressure contours for the upper surface of rigid wing, Liu [11].....	56
Figure B.8 : Pressure coefficients for the elastic wing at 34% span, Liu [11].....	57
Figure B.9 : Pressure coefficients for the elastic wing at 34% span, present study...	57
Figure B.10 : Pressure coefficients for the elastic wing at 67% span, Liu [11].....	58
Figure B.11 : Pressure coefficients for the elastic wing at 67% span, present study.	58

STEADY-STATE AEROELASTIC ANALYSIS AND NUMERICAL DESIGN OPTIMIZATION OF AIRCRAFT STRUCTURES

SUMMARY

Recent advances in aeroelasticity led to multidisciplinary optimization techniques being employed in the field widely. In this work, a generic aircraft wing has been optimized to find the optimum thicknesses of structural members by using commercial codes. Using a commercial software, which utilizes a gradient based algorithm to find sensitivities, an optimal design set has been obtained. However, since the commercial software utilizes finite differencing scheme, it was concluded that analytical sensitivities can be used to decrease computational costs.

To form a basis for an analytical sensitivity based optimization study, a benchmark wing configuration, AGARD 445.6, was selected from the literature and an academic code was used to perform a steady-state aeroelastic analysis of the wing. Finite element code was modified to support modelling the orthotropic wing and to provide a general finite element for sensitivity analysis. Modal structural and steady-state aerodynamic analyses were done to validate the structural and flow models. Finally, steady-state aeroelastic analysis was performed and the result was compared to the existing literature. It was concluded that results compared well. It is the aim of this study that the finite element added will be used to perform sensitivity computations as further study.

UÇAK YAPILARININ DAİMİ REJİMDE AEROELASTİK ANALİZİ VE SAYISAL TASARIM OPTİMİZASYONU

ÖZET

Aeroelastisite alanındaki son gelişmeler nedeni ile çok disiplinli sayısal optimizasyon teknikleri bu alanda genişçe uygulama olanağı bulmuştur. Bu çalışmada bir uçak kanadının yapısal elemanlarının en uygun kalınlık değerlerini elde etmek için optimizasyon yapılmıştır. Gradyan tabanlı algoritmaya sahip bir ticari yazılım kullanılarak oluşturulan metodoloji ile bu kanada ait optimum tasarım kümesi elde edilmiştir. Ancak yazılımın türevleri sonlu farklar yöntemi ile elde etmesi sebebiyle çözüm zamanının arttığı gözlenmiştir. Çalışmadan hesaplama zamanını azaltmak için analitik türevlere ihtiyaç duyulduğu anlaşılmıştır.

Daha sonra yapılacak analitik hassaslık tabanlı bir optimizasyon çalışmasına temel oluşturmak için literatürden deneysel bir kanat konfigürasyonu olan AGARD 445.6 seçilmiş ve bu kanadın statik aeroelastik analizini gerçekleştirmek amacı ile akademik yazılım kullanılmıştır. Kanat konfigürasyonunu modelleyebilmek için ortotropik sonlu eleman desteği yazılıma eklenmiştir. Yapı ve akış modellerini doğrulamak için ise yapısal modelin modal analizi ve akışkan modelinin daimi şartlarda analizleri gerçekleştirilmiştir. Son olarak statik aeroelastik analiz gerçekleştirilmiş, elde edilen sonuçların literatür ile uyumlu olduğu gözlenmiştir. Bu çalışmanın amacı eklenen sonlu elemanın ilerideki bir çalışmada malzemeye bağlı analitik türevlerinin alınarak sayısal optimizasyonun gerçekleştirilmesidir.

1. INTRODUCTION

Aeroelasticity has rapidly become a major field in aircraft design. The nature of the aeroelastic problem requires high-fidelity software for solution which needs high computational capabilities. Moreover, recent advances in the numerical optimization techniques led to multidisciplinary optimization (MDO) studies increasing the need for computational power. In fluid-structure interaction (FSI) problems, nearly all of the MDO studies are reported in the field of aeroelasticity [49].

1.1 Purpose and Outline of the Thesis

One of the solutions to decrease the computational costs for MDO in aeroelasticity is to use gradient based optimization algorithms. These require semi-analytical differentiations where finite difference is used only if necessary.

One of the purposes of this thesis is to perform a study based on gradient-based optimization algorithms. For this purpose, different packages of commercial software were used to numerically optimize a generic aircraft wing with a gradient based algorithm.

Another purpose of this thesis is to form a framework for a CFD based MDO analysis. For this purpose, as a benchmark case, an experimental wing is chosen and a general finite element with orthotropic properties has been added to a readily available finite element code to model this wing. The future work of this thesis is to compute semi-analytical derivatives of material properties of the finite element w.r.t design variables. Before such a study is conducted, the finite element code written for this purpose and the aeroelastic model has to be validated. Thus, a steady-state aeroelastic analysis is performed to validate the benchmark model.

2. REVIEW OF AEROELASTICITY AND MDO

2.1 Review of Aeroelasticity

In aircraft design, aeroelastic effects have been a major design driving factor for a long time. The field of aeroelasticity has witnessed the emergence of aeroelastic codes that use different methods to model fluid-structure interaction with better accuracy and efficiency. These methods show diversity since computational aeroelasticity (CAA) deals with coupling both the fluid and structure equations.

Fluid-structure interaction problem formulation is modelled with respect to the problem. As the complexity in the physics of flow and mechanics increase, the equations that will be solved have to be coupled more efficiently and accurately. CAA focuses on coupling these equations to provide accurate results with minimal computational costs. This review makes use of some recently published surveys to show how CAA has changed in methodology. Additionally, prominent work of some authors in the field is examined.

CAA has some intrinsic issues arising from its focus on coupling the equations of several different domains. A major problem is the transformation of physical data such as pressure and displacement field between the two domains. Another one is increased fidelity in flow physics that leads to complex formulations with high computational costs. Different methodologies are employed to tackle such problems. As stated by Smith and Hodges [1] and Kamakoti et. Al. [3], there are three methods of coupling the two physics. The rest of the terminology in present work is based on the context established by these authors.

First of the coupling methods is the fully coupled one where governing equations of the fluid and structure domain is treated as a single set of equations and solved. Usually, structure is simply modelled as plates and beams with analytical equations while a fluid solver using Navier-Stokes equations is employed [1]. Since this method is considered computationally expensive, it is generally used for simple 2D geometries such as beam/plate like structures.

The first of these is the fully coupled method where the governing equations of the fluid and structure domain is written as a single set of equations and solved. Usually, the structural model is simple such as plates and beams while the fluid solver uses Navier-Stokes equations [1]. It is usually considered computationally expensive and generally used for 2D models (such as beams and plates).

The second of these is the closely coupled method that is widely used. In this method, the transformation of the data between two domains is done at different modules and transformed at each step. The flow is usually solved using Euler/Navier-Stokes equations and the solid can be modelled using finite elements such as solids, beams, shells and plates. Since the coupling is done with the transformation of data at each iterative step, the fluid and structural models can be changed according to the model [1]. Closely coupled methods show diversity in approach according to the problem and there are numerous works published in the area.

The last method is the loosely coupled one that is used only for simple problems such as subsonic flow over thin airfoils. The flow is modelled using velocity potential theory/ transonic small perturbation theory while the solid model is usually represented as modal shapes [3]. This method is still widely used in industrial applications as results can be obtained in a short time for even complex problems to get some early insight into the problem.

Another difficulty arises when interpolating/extrapolating the data between models. Such a difficulty can be overcome with an algorithm selected from a number of efficient ones.

This subject is reviewed extensively in [1], [2] and [3]. It can be said a number of efficient algorithms exist for certain types of problems such as multiquadratic biharmonic, spline matrix, geometric conservation law, linear interpolation/extrapolation.

One more difficulty in treating aeroelastic problems is to find a convenient way to provide a robust solution for mesh motion. Large displacements can occur in highly elastic structures. This can be a problem when element quality is decreased or bad elements form which leads to failure of aeroelastic analysis [53]. This problem can

usually be overcome with treating the fluid mesh with rotational and/or translational springs so that mesh motion can be solved as a mechanical problem.

Overall, the problems of computational aeroelasticity include the coupling of the fluid and structure domains, interpolation/extrapolation of transferable data and dynamic mesh generation.

Huttsell and Schuster, et al. [2], evaluated some aeroelastic codes used to solve divergence, flutter, control surface buzz and a number of other aeroelastic problems. One of the codes is CAP-TSD which solves three dimensional transonic small disturbance potential flow equations (inviscid, compressible) for partial and complete aircraft configurations. The structure is modelled as thin plates and represented with modal shapes. No mesh movement is necessary so the code is computationally efficient. Another code is ENS3DAE which uses the Euler/Navier-Stokes equations to solve the fluid. It includes two different turbulence models and uses mode shapes to represent the structure. It incorporates dynamic mesh algorithms and is usually run on an 8-10 processor computer. The last one is CFL3DAE which also solves Navier-Stokes equations and uses mode shapes that represent the structure linearly. The primary difference between CFL3DAE and ENS3DAE is that the first uses finite volumes as the second one uses central finite difference formulation. Several models including an aeroelastically tailored model, an F-15 flutter model and an AV8B wind tunnel model are employed to solve different problems (that has nonlinear behaviours) and evaluate the codes. The results obtained are in favor of CAP-TSD for simple geometrical and physical models. Otherwise, CFL3DAE is more robust since it has more recent mesh and turbulence formulation with a better algorithm. However, it is suggested the Euler/Navier-Stokes solution of the flow should be limited to static phenomena since it is computationally expensive for dynamical problems.

Dowell, Carlson et al. [4] suggested two different reduced-order models for highly nonlinear aeroelastic problems. These methods are the proper orthogonal decomposition method which is analogous to structural modes and the harmonic balancing model which involves solving the Navier-Stokes or Euler equations without having to integrate time integrations to predict dynamic behaviour. The two models are solved for the flow over a cylinder and the results are compared. The results show good agreement with the experimental data.

Farhat [5] addresses some issues related to computational problems in aeroelasticity. He concluded that the stability of arbitrary Lagrangean/Eulerian formulation of Navier-Stokes or Euler equations is proved and a mature way to represent dynamic meshes. It is also suggested that the spring method or corotational method is used as mesh deformation algorithms. The AERO code which is presented as an example of the mentioned accomplishments proved to solve a complete aircraft configuration giving valuable insight to aeroelastic problems.

In their study, Gordnier et al. [6], a nonlinear structural solver is coupled with a Navier-Stokes solver to model aeroelastic effects on an isotropic plate. The finite element model is based on the von Karman plate equations for an isotropic plate and the mesh is of uniform elements with four nodes. The structural solver is first validated for both clamped and pinned models, then the aeroelastic problem of the plates are solved. It is stated that the results are in good agreement with experimental data.

Lohner et al. [7] has addressed the coupling issue and suggested using ALE scheme for discretization of the fluid/structure domain and obtains efficient dynamic meshes. Attention is also directed to some drawbacks of the ALE formulation in certain cases.

Massjung [8] used 2D Euler and von Karman equations for fluid and structure modelling respectively for solving flutter and bifurcation problems. The domains are discretized with a so called “energy budget of the continuous problem” method and predictor strategies and fixed-point iterations are employed for coupling. The method is validated for the aeroelasticity of a plate. It is also shown that the discrete geometric conservation law for predicting the stability of dynamic grids proposed by Farhat and Lesoinne is in compliance with the energy method used. The results show that the convergence of the solution is directly dependent on the time step taken.

Newman, et al. [9] has done a nonlinear aeroelastic wing analysis solving nonlinear Euler equations for subsonic, transonic and supersonic flows. The structure is modelled with tetrahedrons allowing complex geometries. A convergence criterion is established with “interaction analysis control” where the interaction between two domains is terminated when this criterion is satisfied. As a result, only 10% more time is required for solving when compared to static wing analysis. It is also noted

that unstructured solid mesh allowed observing the stress gradients along the structure which is impossible with modal representation.

In Suleman et al. [10], modelled the structure with corotational finite element theory and a staggered algorithm (improved serial staggered) proposed by Farhat and Lesoinne is used. The results show that the corotational theory can predict the limit cycle oscillations that are related with geometric nonlinearities which otherwise is predicted as unstable behaviour when linear structural models are used.

Liu et al. [11], performed the static aeroelastic computation for the AGARD wing. The structural model is represented as modal shapes and the flow is solved with Euler/Navier-Stokes equations. The interpolation between the moving grids is achieved with spline matrices. The original code used (ACES3D) is originally designed for solving dynamic behaviour so the code is modified so that time-accurate terms are ignored. This approach is disadvantageous if large deformations occur so a relaxation method is employed to make the solution converge for these geometries. The code partitions the flow domain into multiple blocks that are distributed over a number of parallel processors so that computational efficiency is maintained. The results show that only 10% more time is needed for static aeroelastic solution when compared to a rigid solution. The relaxation method proves to be useful to make the solution converge when the model endures large deformations.

Guruswamy et al. [12], investigated the divergence speed and aileron reversal problems for a wing with a control surface. The flow is solved by using Reynolds averaged Navier-Stokes (RANS) formulation while the aeroelastic equations of motions is solved using Rayleigh-Ritz method which uses assumed modes to find aeroelastic displacements. The flow equations are solved by using an upwind differencing scheme. From the results, it is shown that in the transonic regime the Navier-Stokes equations could predict the aeroelastic behaviour well though a better turbulence model could lead to better predictions.

Relvas and Suleman [13] employed the nonlinear corotational theory to account for large displacements and adopted the staggered aeroelastic procedure proposed by Farhat and Lesoinne [57] to solve the aeroelastic problem.

An integrated solution method is proposed by Newmann and Newman et al. [14] such that the fluid and structure equations are solved separately and matched at

boundaries. The method is compared to domain decomposition methods which utilize several domains while the present approach only employs two domains (fluid and structure) and interfaces them at the boundaries of these two domains (i.e.: the surfaces of the structures). The structure and the flow are modelled with finite elements and the Euler equations. The aerodynamic forces are transferred at the boundaries of the domains by using lumped forces technique. The configuration is a full aspect ratio wing with a truss frame. Spring method is used to move the surface mesh. System convergence criterion is the rms of the wing surface deflections. The analysis is run for three different flow conditions including subsonic, transonic and supersonic and loss of lift is observed especially for the transonic case.

Karpel [15] solved dynamic equations for the modal representation of the structure by having the solution converge to steady state by introducing an artificial structural damping. The configuration is a rocket with fins at the back. Euler equations are solved for inviscid flow. Modal equations are used to overcome the singularity problem in a free-free configuration. The analysis is run for a stream speed of 3.5 Mach and an angle of attack of 5 degrees. The results show that while the aeroelastic deflections can be neglected, the lift distribution and moment coefficient changes significantly.

Schuster [16] performed the static aeroelastic analysis of an aeroelastically tailored wing. The aim is to predict vortices, shock waves, separated flow in an unsteady flow using Navier-Stokes equations. The code used includes its own grid generating technique which is called zonal grids. Either the influence coefficient or modal equations can be used to solve for static aeroelastic deflections. It is argued that though the influence coefficient model demands much more memory and storage (convergence requires more grid points) when compared to modal equations, the influence coefficient model gives more reliable results and worth the extra time. A simple algebraic method is used to deflect the grid. The pressure coefficients and aeroelastic deflections are calculated. The results show that the turbulence model (Baldwin-Lomax model) used predicts the flow separation location aft when compared to the experimental data. The pressure coefficients seem to correlate with the experimental pressure coefficients.

In the study of Liu et al. [17], the closely coupled method utilizes multiple grids and multiple domains to predict static aeroelastic behaviour. The grids are interfaced

using the spline matrix interpolation method. The test case is a cantilevered wing (AGARD 445.6). The spring method is used to deflect the grids and the code is parallelized using domain decomposition. Modal equations are used to solve static deflections by using an artificial structural damping ratio that forces the system into steady state. The method proposed works in case of small deformations, but for large deformations a relaxation procedure is utilized to overcome convergence issues. Both the Euler and Navier-Stokes equations are used to solve the flow and the solutions are compared. Significant differences between the two solutions arose such as flow separation prediction, twist and pressure coefficients.

In Guruswamy et al.'s [18] work an arrow-like experimental configuration is used for unsteady transonic static aeroelastic computations. Both rigid and flexible solutions are obtained and compared. The effect of flap deflection on the aeroelastic characteristics is considered. An artificial damping term is introduced to dynamic modal equations to converge the solution to steady state forcefully. The wing is modelled as a flat plate and aeroelastic deflections at various stations along the span and pressure distribution are evaluated. The results show that significant lift loss (compared to rigid solution) related with aeroelastic behaviour is observed. It is concluded that the computed solution correlates well with the experimental data.

Guruswamy et al. in their study argued that the use of wing box structure made modal equations impractical since it would be difficult to find a mode shape compatible with the aeroelastic deflection of the structure that includes a wing box [19]. Instead finite element analysis is employed using different kind of elements. Further, the structure can have composite material properties which would be difficult to implement with modal representation. The in-plane motions of the membrane elements used to model panels are neglected, a so called static condensation method is used and chord wise rigidity is assumed to decrease computation time. Several schemes for transferring aerodynamic loads on the structure are proposed in the work. It is concluded that promising static aeroelastic results are obtained and the most important outcome of the work is assumed to be the usage of full finite element model which is advantageous since stress distribution is also obtained for the structure.

Kamakoti et al. developed a pressure based solver for aeroelastic problems [20]. Full Navier-Stokes is solved for the AGARD 445.6 wing model and a membrane model

without compressibility effects. The membrane structure is modelled using shell elements using hyperelastic Mooney's law. Multiple grids are used to solve structure and fluid equations and the interfacing is done with linear interpolation and extrapolation. The domain is divided into blocks for parallelization and new methods such as numerical diffusion for convection and pressure terms are used. As the turbulence model, the widely used k- ϵ model is adopted. The aerodynamics is solved to obtain pressure on surface of the structure so that these values are converted to nodal forces acting on the structure. As in similar studies, the cross section of the AGARD wing is assumed to be rigid which leads to easy prediction of twist and span wise deflection. Pressure distribution and aeroelastic deflections are computed for both of the models.

Farhat and Lieu [24] modelled the flow with proper orthogonal decomposition (POD) to reduce the order of magnitude of flow equations. By changing Mach number and angle of attack, effect of these changes on POD model was inspected. This reduced order model was applied to a full aircraft configuration. Good correlation is claimed between the full order analysis and the reduced order analysis in the transonic regime.

In the last 20 years, significant advances have been gained in the field of aeroelasticity as seen from above studies. The first studies generally aimed at solving the flow around a rigid structure. (These studies were not included in the review.) With more computational power, the theory of the solvers shifted from the simple models such as transonic disturbance model to Euler and/or full Navier-Stokes equations with turbulence models. This led the way to predict complex flows with turbulence, flow separation, viscosity, compressibility etc. After these studies, the time had come to inspect the fluid-structure interaction. In the first years of the field, simple structural models were used to predict static elastic deflection. As more computational is gained in time, finite element analysis for complex structures became more favoured. Later on, the work was more focused on the problems of aeroelastic modelling such as the interfacing of the fluid and structure domains, faster algorithms for solving the flow and structure equations, algorithms for grid generation and deflection, grid generation for complex models.

As the number of solvers increased, the need for experimental data arose to validate these codes. The result is the wind-tunnel models specifically designed to collect data

related with flow and aeroelastic behaviour. The most used and widely known ones are the AGARD 445.6 aeroelastic configuration, the aeroelastic research wing and an arrow-like configuration [21, 22, 23] .

Table 2.1: Methodology Comparison in CAA

<u>Author</u>	<u>CFD Solver</u>	<u>Structural Solver</u>	<u>Moving Mesh Algorithm</u>	<u>Interfacing Method</u>
Cunningham et al (1988) [20]	TSD	Modal	none	None
Robinson et al. (1991) [20]	Euler	Modal	Spring Method	None
Lee-Rausch and Batina(1993) [20]	Navier-Stokes	Modal	Spring Method	None
Soulaimani (2000) [20]	FEM Based	(Commercial)	ALE	None
Liu, et al. (2000) [17]	Euler	FEA	TFI	Spline method
Farhat and Lessoine (2000) [20]	Navier-Stokes	FEA	ALE	Conservative geometric law
Kamakoti et. al. (2002) [20]	Navier-Stokes	Bernoulli-Euler Beam	TFI	Linear Interpolation & Extrapolation
Guruswamy et. al. 1994 [19]	Navier-Stokes	FEA	Grid Generation	Local Conservation Scheme
Newmann et. al. 1999 [9]	Euler	FEA	Spring Method	Lumped forces technique
Liu et. al (1993) [11]	Euler or Navier-Stokes	Modal	Grid remeshing	Spline Method
Schuster et. al. 1990 [16]	Euler or Navier-Stokes	Influence Coefficient or Modal	Algebraic Shearing	None
Lieu and Farhat [24]	Navier-Stokes with POD	FEA	ALE	Conservative geometric law

Some of the work in the field of aeroelasticity is summarized in Table 2.1. It includes the details such as the fluid and structure model, interfacing technique, grid moving method etc.

2.2 Review of MDO

In recent years, design optimization of complex aircraft structures for maximum performance and minimum cost has been a challenging research area for aircraft manufacturer companies. The multi-objective task of attaining minimum weight and cost with maximum reliability of structure is one of the most time-consuming phases of an aircraft design project. Therefore, robust computational methodologies are strongly required in order to increase the efficiency and success of this design phase. A strong and easy-to-apply methodology can be developed by implementing the numerical optimization techniques directly into the everyday-used analysis tools that have been well and commonly employed in aerospace engineering. Numerical optimization is an iterative scheme to reach the most desired design within a design space bounded by the lower and upper limits of optimization variables. The design criteria, defined as functions of optimization variables, have to be evaluated at each optimization iteration as variables are updated. Thus, optimization studies require a high number of sequential analyses automatically and needs longer computational time as compared to only analysis studies. For that reason, a serious research is focusing on developing more efficient optimization algorithms for problems with large analysis size. For only optimization purposes simpler analysis models can be preferred in the iterative process and parametric geometries can be used to reduce the number of optimization variables that can sufficiently describe a problem. In literature, for the structural analysis component of aircraft wing multi-disciplinary optimization, mostly simple structural models are employed. Bowman et al. [30] used finite element analysis with bars, panels, and membranes to model the wing as a rectangular prism with a constant chord. In order to model a helicopter rotor blade, Friedman [32] used finite element analysis for thin walled, rectangular box sections representing the structural member at each span-wise station. Barthelemy et al. [27] and Dovi et al. [31] used an equivalent laminated plate formulation to model aircraft wings by the trapezoidal plates. Jha and Chattopadhyay [36] modelled the wing configuration of a high speed business jet with a rectangular box beam with taper and sweep and used a panel code as the flow solver. Meanwhile, the validity of the results obtained by using these simple models have been increasingly questioned as advanced structural analysis methods have been developed. Tzong et al. [42] and Maute et al. [38] used high fidelity structural codes for coupled optimization.

Optimization problems can be solved by a broad range of algorithms which can be classified into two main groups as gradient-free algorithms and gradient based algorithms. As examples of gradient-free algorithms, genetic algorithms and evolutionary strategies provide the most robust tools to find the global optimum (Goldberg [33], Grierson and Hajela [34], Back [26]). However, these algorithms require a large number of function evaluations that may be computationally expensive. On the other hand, when the optimization criteria are sufficiently smooth functions of optimization variables, the gradient based methods are computationally more efficient since they require only a few function evaluations. However, they require evaluating the gradients of the optimization criteria. These gradients of the optimization criteria with respect to the optimization variables are called sensitivities and can be found either by finite differencing (numerical methods), complex-step or by analytical sensitivity analysis. Different first order and second order algorithms can be used to determine the search direction such as Steepest Descent, Conjugate Gradient, Newton Method (and Quasi-Newton methods DFP ve BFGS), Sequential Quadratic Programming (SQP and NLPQL [40]) . Some examples to gradient-based optimization applications in aircraft design are work of Baysal and Eleshasky [28], Giunta [35], Kirsch [37], Bendsoe [29] , Maute [39], and Nikbay [40] .

These numerical methods are increasingly being used in multidisciplinary problems such as aeroelasticity. Since multidisciplinary analyses are computationally expensive, to find optimum solution at a relatively lesser cost, either the governing equations are kept simple or gradient based methods are employed. Early MDO work in aeroelasticity usually involves eliminating instabilities by modelling the physical problem with simple flow/structural equations and solving the optimization problem while recent work focuses on problems with more complex physics.

Kolonay [43] employed nonlinear transonic small disturbance to solve flow physics and used gradient based sensitivities to find optimum flutter speed of a rectangular wing. It was concluded that nonlinear theory yielded significantly different results when compared to linear flow equations. Bowman [30] used strip theory for modelling aerodynamics and tried to alleviate control reversal and divergence by evaluating gradient based sensitivities of divergence speed and lift. Delaurentis et al. [44] employed Design of Experiments/Response Surface Methods to find a balance between computational cost and higher fidelity. Battoo [45] optimized a 600 seat

aircraft with large numbers of constraints to maximize flutter speed by employing linear aerodynamics and simple finite elements. Thickness distributions were optimized to find a structure with a constrained weight. More recent work includes Ricci's [46] where a morphing wing is optimized for minimum weight under aerodynamic load and constrained by material strength. Martins et. Al. [47] proposed using coupled sensitivities to optimize a complete wing configuration by Euler equations for aerodynamics and detailed finite elements for structural analysis thus maintaining higher fidelity. Epstein [48] employed genetic algorithms (GAs) as an optimization tool in combination with a reduced-order-models (ROM) method, based on full Navier–Stokes computations. It was reported that considerable aerodynamic efficiency was gained. In conclusion, as Guruswamy [49] reports, general trend in aeroelasticity is to preserve high fidelity in modelling physics while using gradient based optimization algorithms. It was also pointed out that all of the high fidelity optimization techniques in MDO were done in the field of aeroelasticity.

3. NUMERICAL DESIGN OPTIMIZATION

A generic optimization problem associated for a given system can be formulated as [25]:

$$\begin{aligned} \min_{s \in S} z(s) \\ h(s) = 0, h(s) \in R^{n_h} \\ g(s) \leq 0, g(s) \in R^{n_g} \\ S = \{s \in R^{n_s} \mid s_L \leq s \leq s_U\} \end{aligned} \tag{3.1}$$

where s is a set of n_s abstract parameters restricted by lower and upper bounds s_L and s_U , z is a cost function of interest, h denotes a set of n equality constraints, g is a set of n_g inequality constraints. The physical design parameters can be defined as functions of the abstract optimization variables s . In this work, the optimization problem will cover structural type of inputs as the optimization criteria and optimization variables. The structural design parameters can be cross sectional and thickness dimensions of the structural elements and some shape parameters. The optimization criteria h and g can cover the structural behaviour descriptors such as mass, displacements, stresses, strains, and modal frequencies.

3.1 Application of Numerical Design Optimization

We consider multi-objective structural design optimization of a simple aircraft wing which has a NACA0012 airfoil profile [50]. The wing geometric model consists of skin panels, ribs, spars, stringers, and stiffeners while the finite element model is constructed by using shell and beam elements. The aim of this study is to optimize the thicknesses of these structural members and positioning of selected ribs and spars by employing only commercial software for engineering applications. CATIA V5 is used as a parametric 3D solid modeller where as ABAQUS 6.7, structural finite element method solver, is used to compute the structural response of the wing system. As a multi-objective and multidisciplinary optimization driver, commercial

software, modeFRONTIER 4.0, is used for its gradient-based optimization algorithm options.

The optimization problem involves minimizing mass while maximizing first fundamental natural frequency of a wing as a measure of the rigidity. This multiobjective problem has constraints enforced on the mass and frequency as well as the geometrical properties of structural members and the wing's static response. The design variables are chosen as the thicknesses of all structural members and geometric positions of selected rib and spar members. Abstract optimization variables will be introduced to reduce the number of optimization variables which will be still enough to relate the full set of design variables to the optimization criteria and update the geometry.

3.2 Problem Formulation

In the optimization problem, the minimum mass of the wing is the objective function while constraints concerning the maximum displacement and stress of the structure are formed. Thus, optimization problem can be formulated as:

$$\begin{aligned}
 & \min_{s \in S} M(s) \text{ and } \max_{s \in S} f_1(s) \\
 & h(s) = 0, \quad h(s) \in R^{n_h} \\
 & g_1(s) = \frac{u_{\max}(s)}{u_0} - 1 < 0, \quad g_2(s) = \sigma_{\max}(s) \frac{1.5}{\sigma_{yield}} - 1 < 0 \\
 & g_3(s) = \frac{M(s)}{M_0} - 1 < 0, \quad g_4(s) = 1 - \frac{f_1(s)}{f_1^0} - 1 < 0 \\
 & S = \{s \in R^{n_s} \mid s_L \leq s \leq s_U\}
 \end{aligned} \tag{3.2}$$

where M is the total mass, u_{\max} and σ_{\max} is the maximum displacement and maximum von Mises stress of the wing structure and σ_{yield} is the yield strength of the material. $u_0 = 187mm$ and $M_0 = 330kg$ are chosen as reference values from reference wing (explained in the next chapter) to constraint the displacement and mass.

3.3 Structural Analysis Model

A simple aircraft wing which has a NACA0012 airfoil profile is modelled parametrically in CATIA V5. The wing three dimensional geometric model consists

of 90 skin panels, 10 ribs and 4 spars while some of the skin panels are stiffened by stringers along the wing span. The wing has a rectangular planform with 6 m semi-span and 1.6 m chord length. Finite element model of the wing is composed of linear shell and beam elements. The model prepared in ABAQUS (as shown at right in Figure A.2), consists of 17070 linear quadrilateral elements of shell type, 1264 linear line elements of beam type, total element number of 18334 and 16024 nodes, thus 96144 degrees of freedom. As material aluminium is employed with Young's modulus $E = 70GPa$, Poisson ratio $\nu = 0.33$, density $\rho = 2700kg / m^3$, yield strength $\sigma_{yield} = 400MPa$. As a cantilevered boundary condition, all of the degrees of freedom at the root of the wing are set to zero. The aerodynamic load that will be applied to the wing is supplied from a computational fluid dynamics (CFD) analysis performed for the initial design. An Euler inviscid flow analysis by using Fluent commercial software was made for $M = 0.3$ at sea level to have an idea about the total force exerted on the wing. The obtained total lift force of approximately $25000N$ is then expressed as an elliptic lift function which changes along the wing span but assumed to be constant along the chord. A static load analysis of a similar wing structure will be used as a reference to dictate the desired optimization constraints for this study. The structural criteria related to the reference analysis are shown in Table 3.1. The maximum displacement and the stress distribution on the reference wing are shown in Figures A.3 and A.4.

Table 3.1: Structural analysis results of the reference wing

Criteria	Values
Maximum displacement	187 mm
Maximum von Mises stress	202 MPa
Mass	336 kg
First modal frequency	4.35 Hz

3.4 Optimization Variables

The set of design parameters s used for the optimization problem are summarized as follows. Since ribs, spars and skin panels are modelled as shell elements, the thicknesses of these elements and the diameter of the stringers are chosen as design parameters. The thicknesses of spars, ribs and skin panels are divided into three groups along the wing span, introducing 9 design variables. The outer diameter of all

the stringers are kept constant along the span and expressed as only one design parameter while the wall thickness of the stringers are taken as one over third of the outer diameter. In Figure A.1, the structural components of the wing and the thickness parameters related to these components are presented so that each different colour shows a different design parameter.

The computational time that will be spent for optimization will be shortened if the number of optimization variables that will be used in the optimization loop can be reduced by using abstract optimization variables.

Therefore, four abstract optimization variables k_1, k_2, k_3, k_4 will be used to describe 9 design variables related to the thicknesses of all spars, ribs and stringers. The relation between design parameters and abstract optimization variables are as follows;

$$\begin{aligned} t_{A1} &= k_1 k_2 k_3 \tilde{t}_{A1} \\ t_{A2} &= k_2 k_3 k_4 \tilde{t}_{A2} \\ t_{A3} &= k_3 k_4 k_1 \tilde{t}_{A3} \end{aligned} \quad (3.3)$$

where t_{A1}, t_{A2} and t_{A3} are the physical design variables describing the skin panel thicknesses for the three partitions along the span. t_{A1} is chosen to be on the cantilevered side. $\tilde{t}_{A1}, \tilde{t}_{A2}$ and \tilde{t}_{A3} are the reference values of the thicknesses of the three type skin panels which are dictated in the initial wing design. Similarly;

$$\begin{aligned} t_{B1} &= k_1 k_2 k_3 \tilde{t}_{B1} \\ t_{B2} &= k_2 k_3 k_4 \tilde{t}_{B2} \\ t_{B3} &= k_3 k_4 k_1 \tilde{t}_{B3} \end{aligned} \quad (3.4)$$

where t_{B1}, t_{B2} and t_{B3} are the physical design variables describing the spar thicknesses for the three partitions along the span. t_{B1} is chosen to be on the cantilevered side. $\tilde{t}_{B1}, \tilde{t}_{B2}$ and \tilde{t}_{B3} are the reference values for the thicknesses of the three spar partitions which are dictated in the initial wing design. Finally;

$$\begin{aligned} t_{C1} &= k_1 k_2 k_3 \tilde{t}_{C1} \\ t_{C2} &= k_2 k_3 k_4 \tilde{t}_{C2} \\ t_{C3} &= k_3 k_4 k_1 \tilde{t}_{C3} \end{aligned} \quad (3.5)$$

where t_{c1} , t_{c2} and t_{c3} are the physical design variables describing the rib thicknesses for the three partitions along the span. t_{c1} is chosen for the first rib on the cantilevered side. $\tilde{t}_{c1}, \tilde{t}_{c2}, \tilde{t}_{c3}$ are the reference values for the thicknesses of the three different rib groups which are dictated in the initial wing design. In addition, two more design variables, the stringer outer diameter d_0 and the inner wall thickness of the stringer beam t_w are:

$$\begin{aligned} d_0 &= k_4 \tilde{d}_0 \\ t_w &= d_0 / 3 \end{aligned} \quad (3.6)$$

where d_0 is the reference diameter value of the initial wing design. The abstract optimization variables are chosen to be less than one so that the initial rough structure will be forced to get lighter. The lower and upper limits of the abstract optimization variables are determined as:

$$\begin{aligned} 0.8 &\leq k_1 \leq 1.0 \\ 0.6 &\leq k_2 \leq 1.0 \\ 0.4 &\leq k_3 \leq 1.0 \\ 0.2 &\leq k_4 \leq 1.0 \end{aligned} \quad (3.7)$$

In addition, the geometric location of the first four ribs which is the group on the wing root side and the geometric location of the middle two spars are chosen to be variable. The absolute distances from the root to each of the first four ribs are chosen as four optimization variables y_1, y_2, y_3, y_4 . For two middle spars, the ratio of the distance between the leading edge of the wing to the spar divided by the chord length is chosen as two dimensionless optimization variables c_1, c_2 . Thus, 16 independent design variables are introduced in total.

$$\begin{aligned} 500mm &\leq y_1 \leq 800mm \\ 900mm &\leq y_2 \leq 1300mm \\ 1400mm &\leq y_3 \leq 1950mm \\ 2150mm &\leq y_4 \leq 2800mm \\ 0.25 &\leq c_1 \leq 0.45 \\ 0.55 &\leq c_2 \leq 0.75 \end{aligned} \quad (3.8)$$

A rather bulk wing initial design will be given for the optimization problem since abstract variables are chosen as such to reduce the thicknesses in any ways. At the initial configuration,

$$\begin{aligned}\tilde{t}_{A1} &= \tilde{t}_{A2} = \tilde{t}_{A3} = 5mm \\ \tilde{t}_{B1} &= \tilde{t}_{B2} = \tilde{t}_{B3} = 20mm \\ \tilde{t}_{C1} &= \tilde{t}_{C2} = \tilde{t}_{C3} = 16mm \\ \tilde{y}_1 &= 600mm \\ \tilde{y}_2 &= 1100mm \\ \tilde{y}_3 &= 1600mm \\ \tilde{y}_4 &= 2250mm \\ \tilde{c}_1 &= 0.35 \\ \tilde{c}_2 &= 0.65\end{aligned}$$

It is expected that the optimum wing will be thinner such that the structural elements thicknesses decrease from root to tip in order to increase first natural frequency and decrease mass.

3.5 Optimization Methodology

As an optimization driver, commercial software is employed to update the geometry and analysis data in CATIA and ABAQUS and check the given criteria for optimality. There are both gradient-based and gradient-free optimization algorithms available in this driver, but we prefer to run gradient-based algorithm NLPQLP for its well known computational efficiency. Figure A.5 shows the optimization flowchart for the multiobjective problem. In the Design of Experiments (DOE) phase of the optimization, with the given lower and upper bounds of the optimization variables, a number of initial guess points are determined for the gradient based search of the optimum. These values of the variables are transferred to ABAQUS environment and the boundary conditions are dictated and the structure mesh is generated automatically for the analysis. The analysis results for the criteria (mass, stress, displacement, frequency etc.) are monitored by the optimization driver and the design variables are updated along the new search direction and the analysis is repeated automatically many times until optimum point or the maximum number of iterations is reached. modeFRONTIER reads the selected criteria values from the output files that ABAQUS writes.

As a gradient-based optimization algorithm, NLPQL developed by Schittkowski [41], is based on sequential quadratic programming method (SQP) for solving nonlinear constrained optimization problems with differentiable objective and constraint functions. At any iteration, the search direction is the solution of a quadratic programming subproblem. A Lagrange function for the nonlinear constrained optimization problem (defined by Equation 3.9) can be introduced as:

$$L(s, \eta, \gamma) = z(s) + \eta^t h(s) + \gamma^t g(s) \quad (3.9)$$

where η and γ are the Lagrange multipliers for the equality and inequality constraints. The solution of the Karush-Kuhn-Tucker conditions for Lagrange function is same as the solution of the following quadratic optimization problem successively at each iteration “ k ” of the optimization loop.

$$\begin{aligned} \min_{s \in S} \frac{1}{2} \Delta s^{(k)} + g^{(k)} &\geq 0 \\ \frac{\partial h^{(k)}}{\partial s} \Delta s^{(k)} + h^{(k)} &= 0 \\ s_L - s^k \leq \Delta s^k \leq s_u - s^k \end{aligned} \quad (3.10)$$

In NLPQL, $\frac{\partial^2 L^{(k)}}{\partial s^2}$ is usually approximated by a first-order derivative by using BFGS formula. In this work, to find gradients, the central finite differencing scheme with a relative perturbation of 10^{-3} is used. It is the fraction of the variable value that is used to perturb the starting point in order to compute the derivative.

The goal of a multi-objective optimization problem is to find a compromise solution to minimize a multidimensional vector of objective functions such as,

$$\min_{s \in S} z(s) = (z_1(s), z_2(s), \dots, z_{n_z}(s)) \quad (3.11)$$

where n_z is the number of objective functions. The solution concept of optimization problems with multiobjectives is that of Pareto optimality. “A vector of design variables s^* is said to be Pareto optimal if, for any other vector s , either the values of all the objective functions remain the same, or at least one of them worsens compared to its value at s^* ” [51]. Scalarization methods such as weighted sum

method, weighted global criterion method are used to combine the components of the objective function to form a scalar objective function and then use standard single objective methods to optimize the resulting scalar function. In this work, the two objective functions are treated to be equally important.

3.6 Optimization Results

The optimization algorithm derives a merit function from the optimization variables and checks if the convergence criterion is met by evaluating this merit function. In this study, the convergence criterion was $\varepsilon = 0.001$. The multi-objective problem converges to five Pareto optimal designs. The first three Paretos are very close to each other while the last two Paretos are very close to each other as also shown in Table 3.2. The first group gives approximately 15% decrease in mass and 21% increase in frequency while the second group gives an 8% decrease in mass and a 28% increase in frequency with respect to the reference values of 330 kg and 4.35Hz. The design engineer can make a choice among these two designs according to the importance of mass and frequency objectives.

Table 3.2: Pareto set for the problem

Variables & Criteria	Pareto Optimal set				
	1st	2nd	3rd	4th	5th
Rib group 1 (mm)	12.8	12.8	12.81	16	16
Rib group 2 (mm)	14.52	14.53	14.51	12.34	12.34
Rib group 3 (mm)	4.25	4.24	4.24	2.47	2.47
Skin group 1 (mm)	3.63	3.63	3.63	3.86	3.86
Skin group 2 (mm)	1.33	1.33	1.32	0.77	0.77
Skin group 3 (mm)	1.06	1.06	1.06	0.77	0.77
Spar section 1 (mm)	12.8	12.8	12.83	20	20
Spar section 2 (mm)	16	16	16.01	20	20
Spar section 3 (mm)	14.53	14.53	14.53	15.43	15.43
d (mm)	4.38	4.38	4.38	3	3
Rib location 1 (mm)	800	800	800	800	800
Rib location 2 (mm)	1000	1000	1000	1000	1000
Rib location 3 (mm)	1950	1950	1950	1950	1950
Rib location 4 (mm)	2800	2800	2800	2800	2800
Spar location 1 (mm)	0.37	0.37	0.37	0.31	0.31
Spar location 2 (mm)	20.75	0.75	0.75	0.74	0.73
Mass (kg)	282	282	282	303	303
Frequency (Hz)	5.26	5.26	5.26	5.55	5.55
Displacement (mm)	186.9	186.9	186.9	186.9	186.9
Stress (MPa)	203	203	204	265	265
Improvement in mass	-15%	-15%	-15%	-8%	-8%
Improvement in frequency	21%	21%	21%	28%	28%

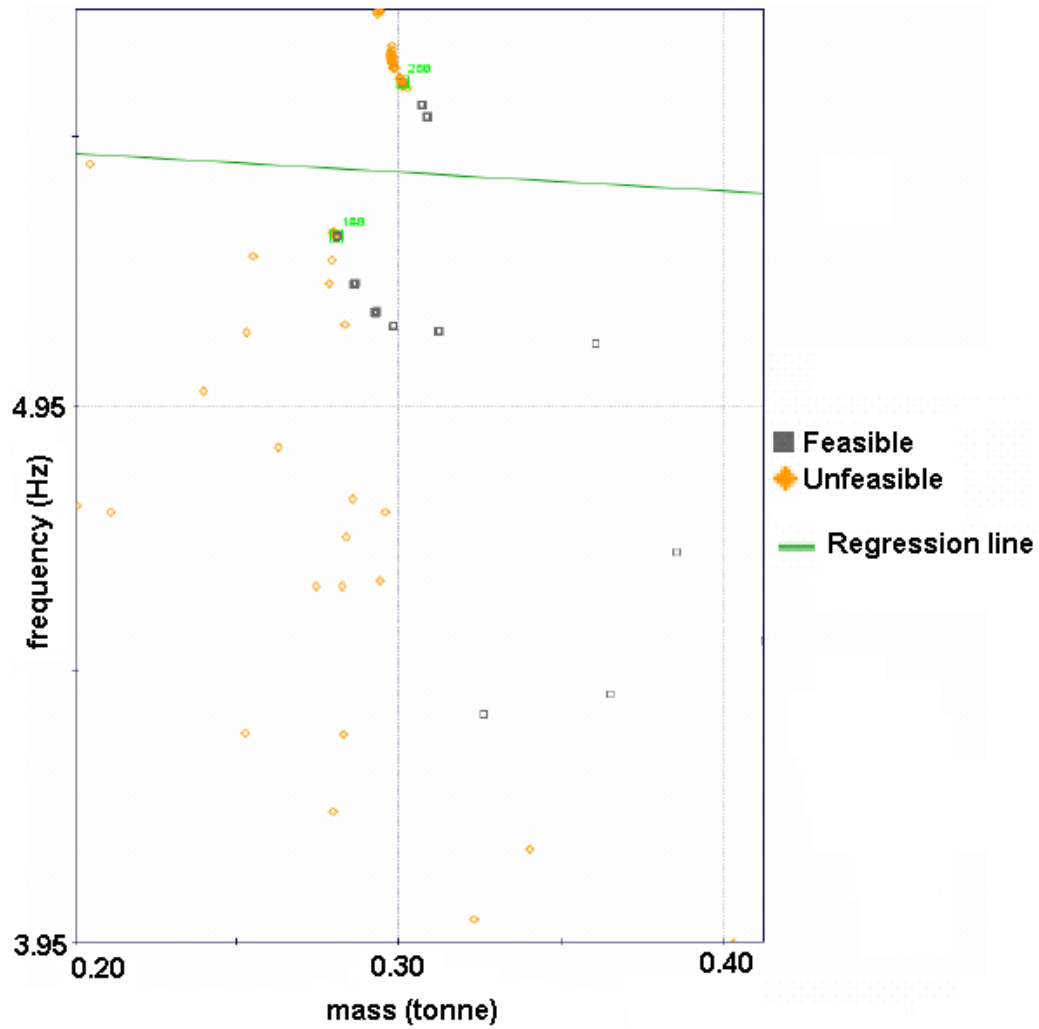


Figure 3.1 : Pareto optimal solution graph

As expected, the optimal set includes designs such that the thicknesses of the structural elements decreased from the root to the tip. In Figure 3.2, it can be seen that the thicknesses decrease from the root to the tip so that first natural frequency can increase and the total mass can decrease.

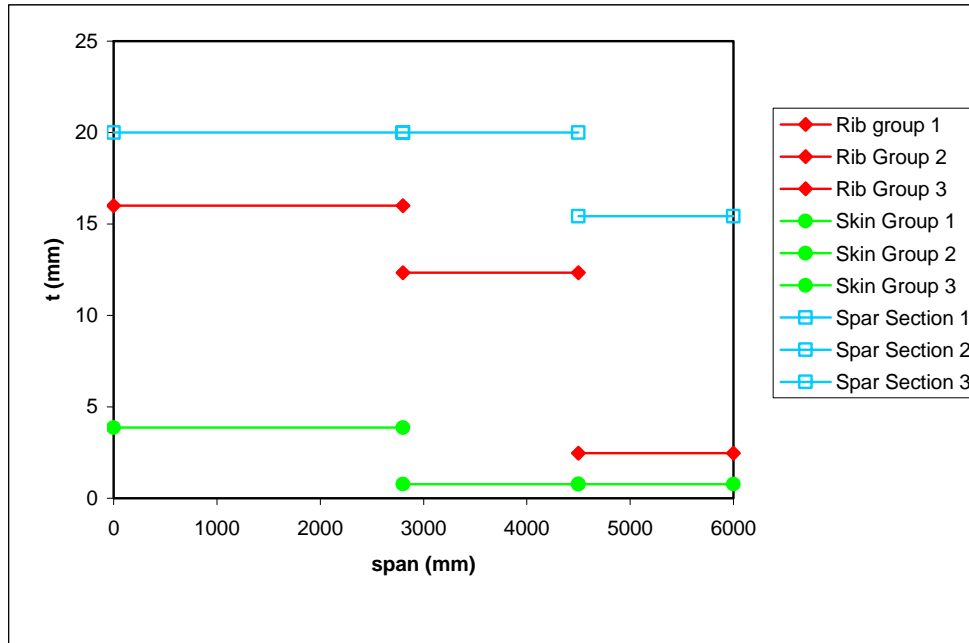


Figure 3.2 : Thickness variation of structural elements along the span

3.7 Conclusion

In this work, a wing structure composed of ribs, skin panels, spars and stringers is successfully optimized. A commercial finite element structural solver, ABAQUS, and commercial multi-objective optimization software, modeFRONTIER, are coupled to demonstrate a practical robust optimization methodology which can be applied in industry. A gradient-based algorithm called NLPQL is used as optimization algorithm and abstract optimization variables are introduced for computational efficiency. The multiobjective problem gave 5 Pareto optimal designs with equal importance level of the two objectives. This result can be further evaluated by introducing significant levels between objectives. For better designs, the number of optimization variables can be increased and also the design variables can also be constrained by considering issues related to manufacturing such as a continuous increase or decrease between consecutive thickness groups making the variables discrete.

This study formed the basis of the framework for a CFD based two way coupled aeroelastic optimization in another study [53]. The logical flowchart used in this

work could be used by replacing structural analysis with an FSI analysis. As a future work, abstract optimization variables will be used for a greater number of design variables and the abstract optimization variables will be chosen by an efficient method.

4. AEROELASTIC ANALYSIS

4.1 Introduction

In MDO review of this work, it was concluded that analytical sensitivities could be used to significantly decrease computational cost of a numerical design optimization. A benchmark configuration in the field of aeroelasticity was selected as a test case to perform a study of MDO by using analytical sensitivities in a future study. For this purpose, AERO suite of open source code was used as an aeroelastic solver. This set of code also includes an optimization library.

To model the benchmark configuration, a general finite element that supports anisotropic material properties has been added to the element library of the structural code of the suite. It is aimed that this element will be used to compute structural sensitivities. However, the finite element and aeroelastic analysis has to be validated first.

To model the structure of the benchmark case, a hexahedral element has been added to finite element library. A brief element stiffness formulation is given in the next chapter. To validate the aeroelastic analysis, the structural and aerodynamic models are validated first. The last chapters are devoted to these studies. Also, general information about the aeroelastic solver AERO-F-S is provided.

4.2 Aeroelastic Solver AERO-F-S

The aeroelastic analysis couples a 3D second-order finite volume Euler code (AERO-F) designed for flow computations on moving grids with Arbitrary Lagrangian Eulerian (ALE) Roe fluxes and with a general purpose finite element structural code (AERO-S or FEM) [53]. This set of codes is the product of collaborative work of various researchers from Colorado University (CU) and INRIA through many years. It was used by Nikbay [38] during doctoral studies in CU. In the present study, the feasibility of further developing AERO-F-S will also be investigated.

In the steady-state aeroelastic analysis, the fluid goes through a transient analysis to reach steady-state solution. The aeroelastic coupling algorithm was based on three-field formulation of Farhat et al. [54] whose discrete form for steady-state can be written as follows

$$\begin{aligned} S(u, x, w) &= 0 \\ D(u, x) &= 0 \\ F(x, w) &= 0 \end{aligned} \tag{4.1}$$

where u is the vector of the structural displacements, x is the mesh motion and w is the fluid state vector. Here, S is the state equation of the structure and can be written as

$$S = Ku - P(x, w) \tag{4.2}$$

Where K is the finite element stiffness matrix associated with the structure, P is the external load vector that combines the aerodynamic load P_T transferred from the fluid to the structure and other specified structural loads such as gravity denoted here by P_o , and can be written as

$$P = P_o + P_T \tag{4.3}$$

The second equation in system 4.1 governs the motion of fluid mesh. Using the spring analogy method proposed by Farhat et al. [55], mesh motion equation can be expressed as

$$\begin{bmatrix} \bar{K}_{\Omega\Omega} & \bar{K}_{\Omega\Gamma} \\ \bar{K}'_{\Omega\Gamma} & \bar{K}_{\Gamma\Gamma} \end{bmatrix} \begin{bmatrix} x_{\Omega} \\ x_{\Gamma} \end{bmatrix} = \begin{bmatrix} 0 \\ \bar{f} \end{bmatrix} \tag{4.4}$$

with

$$x_{\Gamma} = u_T \text{ on } \Gamma_{F/S} \tag{4.5}$$

where u_T is the displacement vector of the grid points on the wet surface of the structure. In equation 4.4, \bar{K} is a fictitious stiffness matrix associated with the fluid

mesh, the subscript Ω designates the fluid mesh points lying inside the fluid domain, the subscript Γ those lying on the fluid-structure interface $\Gamma_{F/S}$ while \bar{f} is the fictitious force needed to enforce equation 4.5. In order to project the structural displacement to the fluid mesh, the displacement projector T_U is defined as

$$u_T = T_u u \quad (4.6)$$

From equation 4.6, it follows that equations 4.4 and 4.5 are rewritten as

$$\begin{aligned} \bar{K}_{\Omega\Omega} x_\Omega + \bar{K}_{\Omega\Gamma} T_u u &= 0 \\ x_\Gamma - T_u u &= 0 \end{aligned} \quad (4.7)$$

Then, x_Γ and x_Ω is computed. Finally, F is the state equation of the fluid and can be expressed as

$$F = F_2(x, w) \quad (4.8)$$

Where F_2 denotes the vector of Roe fluxes resulting from a second-order finite volume discretization of the Euler flow equations.

The three-field formulation outlined leads to a computational strategy that is in general 25% computationally more expensive than a comparable computational method based on a two-field formulation (u, w) of aeroelastic problem [56]. However, most two-field formulations of computational aeroelasticity assume a small displacement field for the structure, and therefore are restricted to few applications. The flow solver AERO is based on Euler equations discretized by finites volumes. In conservative form,

$$\frac{\partial w}{\partial t} + \bar{\nabla} \cdot \bar{F}(w) = 0 \quad (4.9)$$

The fluid state conservative variable, w is defined as

$$w = \begin{Bmatrix} \rho \\ \rho u_1 \\ \rho u_2 \\ \rho u_3 \\ E \end{Bmatrix} \quad (4.10)$$

where ρ is the fluid density, u_1, u_2, u_3 are three velocities and E is the total internal energy per mass. The flux, \vec{F} has three components, $\vec{F}_1, \vec{F}_2, \vec{F}_3$ as follows;

$$\vec{F}_1 = \begin{Bmatrix} \rho u_1 \\ \rho u_1^2 + p \\ \rho u_1 u_2 \\ \rho u_1 u_3 \\ (E + p)u_1 \end{Bmatrix}, \vec{F}_2 = \begin{Bmatrix} \rho u_2 \\ \rho u_2 u_1 \\ \rho u_2^2 + p \\ \rho u_2 u_3 \\ (E + p)u_2 \end{Bmatrix}, \vec{F}_3 = \begin{Bmatrix} \rho u_3 \\ \rho u_3 u_1 \\ \rho u_3 u_2 \\ \rho u_3^2 + p \\ (E + p)u_3 \end{Bmatrix} \quad (4.11)$$

where p is the fluid pressure. Taking integral of equation 4.9 over a control volume C_i in the flow domain and using the divergence theorem gives the fluid equation in continuous form as;

$$\frac{\partial}{\partial t} \int_{C_i} w d\Omega + \int_{\partial C_i} \vec{F}(w) \cdot \vec{\eta}_i d\sigma = 0 \quad (4.12)$$

where ∂C_i is the boundary of control volume C_i centred at vertex "i", $\vec{\eta}_i$ the unit outward normal to the cell boundary, and $d\sigma$ is the differential area. Assembling all the control volumes in the fluid mesh gives equation 4.13 in discrete form as,

$$\frac{d}{dt} (Vw) + \vec{F}(w, x) = 0 \text{ in control volume } \Omega \quad (4.13)$$

Where V is diagonal matrix of cell volumes, w the discretized fluid state variables vector of size $5 \times n_s$, where n_s is the total number of the vertices in the fluid mesh, and x the grid point coordinates vector of size $3 \times n_s$. The numerical flux \vec{F} approximates the integral of the physical flux function over the cell interfaces.

The three-way coupled system of equations 4.1 can be solved efficiently by an iterative staggered procedure that allows the usage of three different solvers, each tailored to each different subproblem [57]. A staggered algorithm is employed. It is graphically depicted in Figure 4.1 where superscript (n) denotes the iteration number.

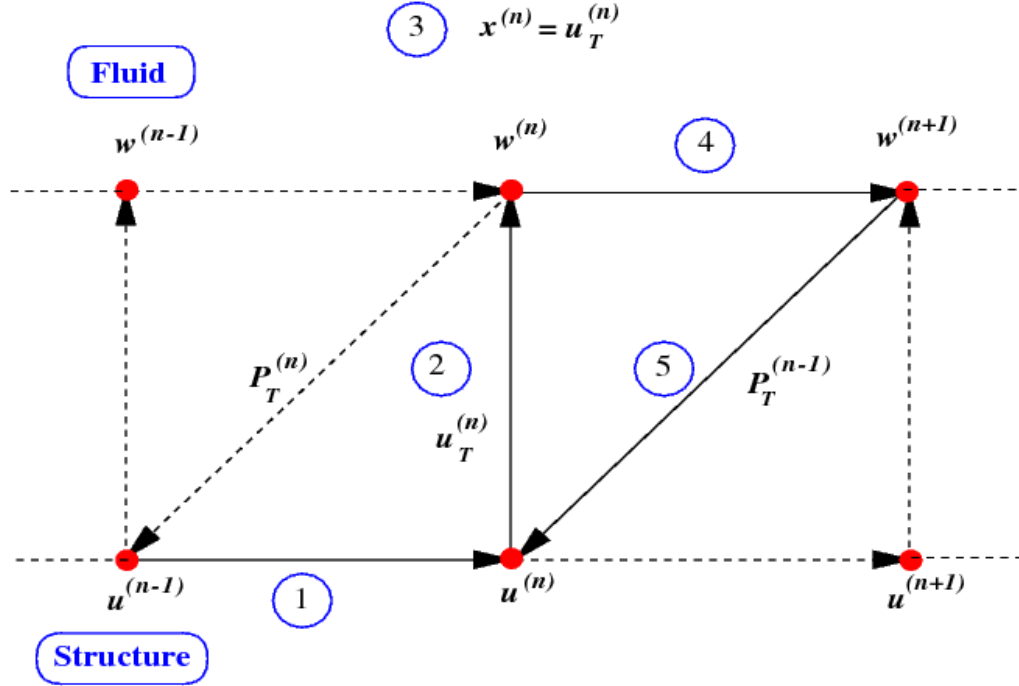


Figure 4.1 : Staggered algorithm for computation of the aeroelastic steady-state

1. For a given external load $P^{(n)}$, determine the structural response $u^{(n)}$ by solving equation 4.2. Then, for numerical stability purposes, perform the following under relaxation

$$u^{(n)} = (1-\theta)u^{(n-1)} + \theta\tilde{u} \quad (4.14)$$

where

$$\tilde{u} = K^{-1}P^{(n)} \quad (4.15)$$

and $0 \leq \theta \leq 1$ is the relaxation factor.

2. Transfer the motion of the wet surface of the structure to the fluid system: $u^{(n)} \rightarrow u_T^{(n)}$. The general relation between $u_T^{(n)}$ and $u^{(n)}$ can be written as

$$u_T^{(n)} = T_u u^{(n)} \quad (4.16)$$

where T_u is a transfer matrix that accounts for potentially non-matching fluid and structure meshes [58].

3. Update the motion of the fluid mesh by solving equation 4.15;

$$\bar{K}x^{(n)} = \begin{bmatrix} 0 \\ \bar{f} \end{bmatrix} \text{ with } x^{(n)} = u_T^{(n)} \text{ on } \Gamma_{F/S} \quad (4.17)$$

Hence, x is updated by setting

$$x_\Gamma^{(n)} = T_u u^{(n)} \quad (4.18)$$

and solving;

$$\bar{K}_{\Omega\Omega} x_\Omega^{(n)} = -\bar{K}_{\Omega\Gamma} T_u u^{(n)} \quad (4.19)$$

Equation 4.18 is solved for mesh motion, $x_\Omega^{(n)}$, with Preconditioned Conjugate Gradient (PCG) algorithm by applying a few iterations so that a valid mesh update which does not produce penetrating elements.

4. Compute the new fluid state vector $w^{(n+1)}$ by applying a single Newton-Raphson subiteration to third equation of the set of equations 4.1. The steady state equation is solved with the following approach;

$$V \frac{w - w^{(n)}}{\Delta\tau^{(n)}} + F_2(w, x) = 0 \quad (4.20)$$

where V is the matrix of cell volumes and $\Delta\tau^{(n)}$ is the pseudo time-step.

5. Extract the fluid pressure $p^{(n+1)}$ on the fluid/structure interface $\Gamma_{F/S}$, compute the aerodynamic load $P_F^{(n+1)}$ by integrating the fluid pressure over $\Gamma_{F/S}$, and transfer the following load to the structure.

$$P_T^{(n+1)} = T_p P_F^{(n+1)} \quad (4.21)$$

where T_p is a transformation matrix that accounts for potentially non-matching fluid and structure meshes. Here, T_p is constructed according to the conservative load transfer algorithm described in [54] and therefore satisfies;

$$T_p = T_u^t \quad (4.22)$$

6. Solve the structure subsystem for $u^{(n+1)}$ and under-relax the solution with

$$\theta^{(n)} u^{(n+1)} + (1 - \theta^{(n)}) u^{(n)} \quad (4.23)$$

where $\theta^{(n)}$ is the relaxation factor at n^{th} iteration.

7. Transfer the relaxed displacement of wet surface to the fluid mesh at surface and solve for the new mesh motion. Check for convergence of the aeroelastic steady-state.

The above staggered algorithm can be described as a block Gauss-Seidel method. The convergence is checked by monitoring the relative residuals of the structure and fluid subproblems and requiring simultaneously.

$$\|S(u^{(n+1)}, x^{(n+1)}, w^{(n+1)})\|_2 \leq \varepsilon^{AA} \|S(u^{(0)}, x^{(0)}, w^{(0)})\|_2 \quad (4.24a)$$

$$\|F(x^{(n)}, w^{(n+1)})\|_2 \leq \varepsilon^{AA} \|F(x^{(0)}, w^{(0)})\|_2 \quad (4.24b)$$

where ε^{AA} is a specified tolerance, and the superscript *AA* stands for Aeroelastic Analysis. Note that only the first inequality (4.24a) assesses the convergence of the proposed staggered procedure. The second inequality (4.24b) emphasizes the importance of requiring that the flow solver converges to the same precision as that imposed on the staggered algorithm.

4.3 Implementation of Finite Element Model with Orthotropic Properties

A brick element with anisotropic material support is implemented to the element library of the finite element code AERO-S. Since this element is a general solid element, it can be used to perform a gradient based optimization of a complex

geometry. This element will be used to model an orthotropic wing and make a steady-state aeroelastic analysis.

An 8 noded, isoparametric, hexahedral element is added to the element library. It has 3 translational d.o.f's per node with a total of 24 dofs as seen in Figure 4.2.

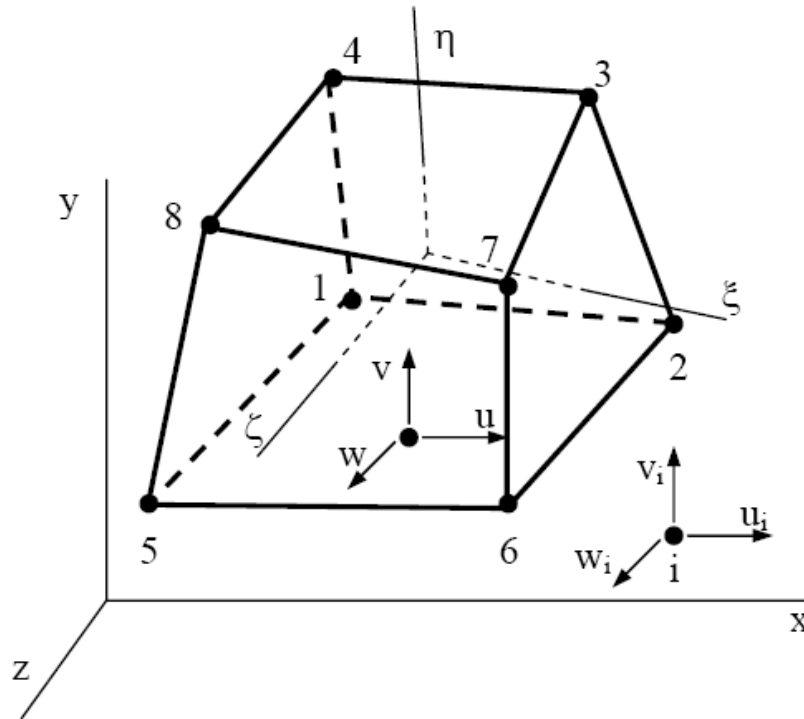


Figure 4.2 : 8 noded hexahedral element

A summary of element stiffness formulation is as the following [59].

The strain-displacement relationship is;

$$\{\varepsilon\} = [d]\{u\} \quad (4.25)$$

Here $[\varepsilon]_{6 \times 1}$ is the strain, $[d]_{6 \times 3}$ is the strain-displacement operator, $[u]_{3 \times 1}$ is the displacement and defined as;

$$\{\varepsilon\} = \begin{Bmatrix} \varepsilon_{11} \\ \varepsilon_{22} \\ \varepsilon_{33} \\ \varepsilon_{12} \\ \varepsilon_{23} \\ \varepsilon_{31} \end{Bmatrix}, \quad \{u\} = \begin{Bmatrix} u \\ v \\ w \end{Bmatrix}, \quad d = \begin{bmatrix} \partial/\partial x & 0 & 0 \\ 0 & \partial/\partial y & 0 \\ 0 & 0 & \partial/\partial z \\ \partial/\partial y & \partial/\partial x & 0 \\ 0 & \partial/\partial z & \partial/\partial y \\ \partial/\partial z & 0 & \partial/\partial x \end{bmatrix} \quad (4.26)$$

If $\{\sigma\}_{6 \times 1}$ is stress and $[E]_{6 \times 6}$ is the elastic matrix, the relationship between them is;

$$\{\sigma\} = [E]\{\varepsilon\} \quad (4.27)$$

For an orthotropic material, elastic matrix $[E]_{6 \times 6}$ in terms of engineering constants is;

$$[C] = \begin{bmatrix} 1/E_1 & -\nu_{21}/E_2 & -\nu_{31}/E_3 & 0 & 0 & 0 \\ -\nu_{12}/E_1 & 1/E_2 & -\nu_{32}/E_3 & 0 & 0 & 0 \\ -\nu_{13}/E_1 & -\nu_{23}/E_2 & 1/E_3 & 0 & 0 & 0 \\ 0 & 0 & 0 & 1/G_{12} & 0 & 0 \\ 0 & 0 & 0 & 0 & 1/G_{23} & 0 \\ 0 & 0 & 0 & 0 & 0 & 1/G_{13} \end{bmatrix}, \quad E = C^{-1} \quad (4.28)$$

To define axes rotation, the stress vector is written as stress tensor so that the rotation matrix R is defined such that;

$$[\sigma] = \begin{bmatrix} \sigma_{11} & \tau_{12} & \tau_{13} \\ \tau_{21} & \sigma_{22} & \tau_{23} \\ \tau_{31} & \tau_{32} & \sigma_{33} \end{bmatrix}, \quad [\sigma]' = [R][\sigma][R]^T \quad (4.29)$$

$$[R] = \begin{bmatrix} \lambda_{11} & \lambda_{12} & \lambda_{13} \\ \lambda_{21} & \lambda_{22} & \lambda_{23} \\ \lambda_{31} & \lambda_{32} & \lambda_{33} \end{bmatrix} = \begin{bmatrix} l_1 & m_1 & n_1 \\ l_2 & m_2 & n_2 \\ l_3 & m_3 & n_3 \end{bmatrix} \quad (4.30)$$

Here, l, m, n are directional cosine values defining the axis of rotation. The rotation matrix in compliance with the strain vector can be written as;

$$\{\varepsilon'\} = [T_\varepsilon]\{\varepsilon\} \quad (4.31)$$

$$[T_\varepsilon] = \begin{bmatrix} l_1 & m_2 & n_2 & l_1 m_1 & m_1 n_1 & n_1 l_1 \\ l_2 & m_2 & n_2 & l_2 m_2 & m_2 n_2 & n_2 l_2 \\ l_3 & m_3 & n_3 & l_3 m_3 & m_3 n_3 & n_3 l_3 \\ 2l_1 l_2 & 2m_1 m_2 & 2n_1 n_2 & l_1 m_2 + l_2 m_1 & m_1 n_2 + m_2 n_1 & n_1 l_2 + n_2 l_1 \\ 2l_2 l_3 & 2m_2 m_3 & 2n_2 n_3 & l_2 m_3 + l_3 m_2 & m_2 n_3 + m_3 n_2 & n_2 l_3 + n_3 l_2 \\ 2l_3 l_1 & 2m_3 m_1 & 2n_3 n_1 & l_3 m_1 + l_1 m_3 & m_3 n_1 + m_1 n_3 & n_3 l_1 + n_1 l_3 \end{bmatrix} \quad (4.32)$$

The stress vector is written as $\{\sigma'\} = [T_\sigma]\{\sigma\}$ so that the rotation matrix becomes

$[T_\sigma] = [T_\varepsilon]^T$. The stress and strain vectors in global coordinates become;

$$\{\sigma'\} = [E']\{\varepsilon'\} \rightarrow [T_\sigma]\{\sigma\} = [E'] [T_\varepsilon]\{\varepsilon\} \quad (4.33)$$

If equation 4.33 is multiplied by $[T_\sigma]^{-1}$;

$$\{\sigma\} = [T_\sigma]^{-1} [E'] [T_\varepsilon]\{\varepsilon\} \quad (4.34a)$$

$$[E'] = [T_\sigma][\sigma][T_\sigma]^{-1} \quad (4.34b)$$

The coordinates of a point inside the hexahedral can be written with shape functions as;

$$x = \sum_{i=1}^8 f_i x_i, \quad y = \sum_{i=1}^8 f_i y_i, \quad z = \sum_{i=1}^8 f_i z_i \quad (4.35)$$

$$\begin{aligned} f_1 &= \frac{1}{8}(1-\xi)(1-\eta)(1-\zeta), & f_2 &= \frac{1}{8}(1+\xi)(1-\eta)(1-\zeta) \\ f_3 &= \frac{1}{8}(1+\xi)(1+\eta)(1-\zeta), & f_4 &= \frac{1}{8}(1-\xi)(1+\eta)(1-\zeta) \\ f_5 &= \frac{1}{8}(1-\xi)(1-\eta)(1+\zeta), & f_6 &= \frac{1}{8}(1+\xi)(1-\eta)(1+\zeta) \\ f_7 &= \frac{1}{8}(1+\xi)(1+\eta)(1+\zeta), & f_8 &= \frac{1}{8}(1-\xi)(1+\eta)(1+\zeta) \end{aligned} \quad (4.36)$$

The Jacobian of the element is

$$[J] = \begin{bmatrix} x_{,\xi} & y_{,\xi} & z_{,\xi} \\ x_{,\eta} & y_{,\eta} & z_{,\eta} \\ x_{,\zeta} & y_{,\zeta} & z_{,\zeta} \end{bmatrix} \quad (4.37)$$

The strain-displacement relationship is rewritten as equation 4.34;

$$\{\varepsilon_i\} = [B_i] \{q_i\} \quad (4.38)$$

Here;

$$[B_i] = [d] \{f_i\} = \begin{bmatrix} f_{i,x} & 0 & 0 \\ 0 & f_{i,y} & 0 \\ 0 & 0 & f_{i,z} \\ f_{i,y} & f_{i,x} & 0 \\ 0 & f_{i,z} & f_{i,y} \\ f_{i,z} & 0 & f_{i,x} \end{bmatrix} \quad (4.39)$$

In Cartesian coordinates, the stiffness matrix of the element is;

$$[K] = \int_V [B]^T [E] [B] dx dy dz \quad (4.40)$$

If the elastic constants are constant through the element, In natural coordinates, the stiffness matrix in natural coordinates becomes

$$[K] = \int_{-1}^1 \int_{-1}^1 \int_{-1}^1 [B(\xi, \eta, \zeta)]^T [E] [B(\xi, \eta, \zeta)] |J(\xi, \eta, \zeta)| d\xi d\eta d\zeta \quad (4.41)$$

4.4 Model Validation

The well-known AGARD (Advisory Group for Aerospace Research and Development) 445.6 wing is chosen as the wing geometry for this study. This wing is the first aeroelastic configuration that is tested in the ‘‘Transonic Dynamics Tunnel (TDT)’’ at the NASA Langley Research Centre [21]. The AGARD 445.6 wing is a swept-back wing with a quarter-chord sweep angle of 45 degrees. Cross sections of the wing are NACA 65A004 airfoils. The wing has a taper ratio of 0.66, a span of

0.762 m and an aspect ratio of 1.65. It is a wall-mounted model made with laminated mahogany. In this study, weakened model 3 of the wing is used.

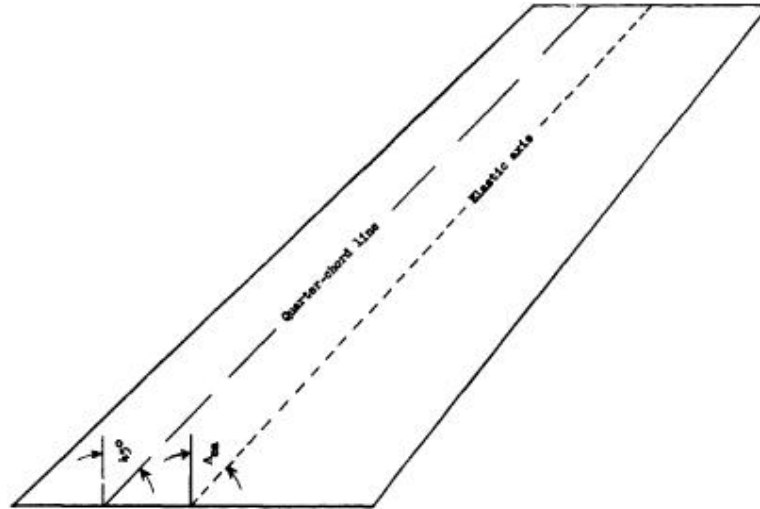


Figure 4.3 : AGARD 445.6 wing geometry

4.4.1 Structural Model Validation

The AGARD wing has experimental data available for validating natural vibration frequencies. A pre-processing tool was not readily available for creating finite element mode so it was formed in ABAQUS by using 14356 linear hexahedral structural elements with 54978 d.o.f's. The material properties of the wing are taken from the work of Yosibash et al [60] for the solid model and modified to represent the weakened model. The modified material properties are shown in constitutive form below.

$$[C] = 10^7 \begin{bmatrix} 46.719 & 1.5197 & 2.1533 & 0 & 0 & 0 \\ 1.5197 & 29.2223 & 15.9277 & 0 & 0 & 0 \\ 2.1533 & 15.9277 & 48.8434 & 0 & 0 & 0 \\ 0 & 0 & 0 & 32.1350 & 0 & 0 \\ 0 & 0 & 0 & 0 & 39.0000 & 0 \\ 0 & 0 & 0 & 0 & 0 & 13.6500 \end{bmatrix}$$

Figure 4.4 : Constitutive matrix corresponding to orthotropic matrix

The wing is clamped at root and a modal analysis is run. The comparison of modal shapes and frequencies are shown in Figure B.1.

Table 4.1: Comparison of calculated frequencies with experimental data

Mode Number	Yates [21] Calculated-Experimental (Hz)	Present Study (Hz)	Error % (w.r.t experimental data)
1 st	9.59-9.60	9.61	0.1
2 nd	38.16-38.10	37.33	2.0
3 rd	48.34-50.70	55.94	10.3
4 th	91.54-98.50	104.12	5.7

Additionally, the mass of the original wing is $1.8627kg$ while mass is calculated to be $1.8609kg$ in the present study. The results show good agreement with the experiments. The first and second modes are pure bending and pure torsion modes while the third and fourth modes are coupled bending/torsion modes as expected.

4.4.2 Aerodynamic Model Validation

Before steady-state aeroelastic is run, the aerodynamic model has to be validated. For this purpose, an unstructured CFD grid with 403321 tetrahedras is prepared with ANSYS ICEMCFD. A simple code was written to convert the aerodynamic grid to AERO format since a pre-processing tool was not readily available. The fluid domain was decomposed into 4 subdomains with TOP/DOMDEC which uses numerical optimization techniques to minimize intercommunication between parallel nodes [61]. A steady-state analysis with Mach number 0.85 and 5 degrees of angle of attack is performed. In Figures B.2 and B.3, CFD grid is seen with boundary conditions.

The steady-state flow analysis results are compared with those from Liu [11]. The pressure contours for the rigid wing are below from the reference work at left and from the present study at right;

The pressure coefficients of upper and lower surfaces at 34% and 67% stations along the span for the rigid wing are compared in Figures B.8, B.9, B.10 and B.11.

The pressure coefficients (c_p) generally agree well with the reference work. For $\xi = 0.34$, Liu [11] predicted a c_p larger than -1.4, while in the present study it is -1.16. At the leading edge, for $\xi = 0.67$, c_p is greater than -1.4 though the present analysis shows a c_p of 1.17. The difference at the leading edge can be contributed to the detailed O-grid mesh used in the reference work whereas in the present study a coarse grid was used.

4.5 Steady-state Aeroelastic Analysis

For the steady state analysis, the CFL number for the flow number is fixed at 100 which is equal to a pseudo time-step size of 0.12×10^{-4} s. The structural time step for the finite element analysis is 0.995×10^{-2} s that is more than 100 times of the fluid time step. The relaxation parameter, fixed at 0.5, is used to prevent divergence that may occur when the initial structural displacement vector is transferred to the fluid mesh.

The aeroelastic convergence criterion ε^{AA} is set to 10^{-8} and the solution converged within 3740 fluid time steps. The solution converged after 3h 36 min wall clock time on 4 Xeon 3.4 GHz processors for the fluid domain and 1 Xeon 3.4 GHz processor for the structural domain.

In Figure 4.5, the deflected wing is shown. The deflections on trailing edge and leading edge at the wing tip are 58.2 mm and 51.3 mm, respectively. The results compare well with the reference work where deflections are about 67 mm and 53 mm.

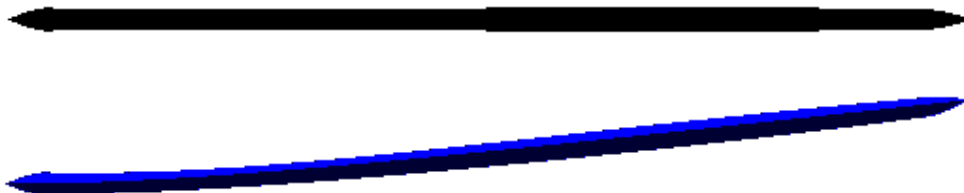


Figure 4.5 : Deflected and undeflected wing

Table 4.2: Displacement comparison at leading and trailing edges

	Displacement (mm) at	
	Leading Edge	Trailing Edge
Liu	53	67
Present Study	51.3	58.2

4.6 Conclusion

Steady-state aeroelastic analysis of an experimental wing configuration is performed. The aerodynamic coefficients generally agree well with the data from literature considering the coarseness of the fluid grid. The deflections obtained are lesser when compared to the reference study. This can be contributed to the pressure coefficients obtained being smaller. As stated by Liu [11], the pseudo time-step approach requires conflicting orders of magnitude in structural and flow time-steps. This results in the solution requiring typically longer computational times (more than a factor of 100) when compared to a fully steady-state analysis which does not take time dependent terms into account. Finally, the finite element was adequate to model complex geometries and will form a basis for sensitivity calculations.

5. CONCLUSION AND FUTURE WORK

A generic wing was parametrically modelled and numerically optimized under design constraints to increase its stiffness. A gradient-based algorithm was used to find optimum thickness values of the structural members. Since commercial software was used to perform the analysis, finite differencing scheme had to be used for evaluating sensitivities of the design variables. It is concluded that analytical sensitivities are advantageous in decreasing the computational time, however open source software has to be generally employed to compute gradient based sensitivities efficiently.

Also, steady-state aeroelastic analysis of an experimental orthotropic wing is performed. In order to model the wing, a hexahedral element has been added to the finite element library of the structural code. After both of the flow and structural models are validated, steady-state aeroelastic response of the wing is obtained. Results show good agreement with the reference work. However, a detailed grid for the flow solver can be used to get better results. Overall, this study can form a basis for computing the sensitivities of the constitutive matrix of a general finite element so that a gradient based optimization is performed.

REFERENCES

- [1] **Smith, J. M, Hodges, H. D.**, Evaluation of Computational Algorithms Suitable for Fluid-Structure Interactions, *Journal of Aircraft*, Vol. 37 No.2, April 2000
- [2] **Huttsell, L., et al.**, Evaluation of Computational Aeroelasticity Codes for Loads and Flutter, *AIAA Journal*, 2001, AIAA-2001-569 Aerospace Sciences Meeting and Exhibit, 39th, Reno, NV, Jan. 8-11
- [3] **Kamakoti, R., Shyy, W.**, Fluid-structure Interactions for Aeroelastic Applications, *Progress in Aerospace Sciences*, 2004. Vol.40, Iss.8, 535-558
- [4] **Carlson, H. A., Feng, Q. J.**, Computational Models for Nonlinear Aeroelasticity, AIAA Paper, *43rd AIAA Aerospace Sciences Meeting and Exhibit*, , p.4143-4152
- [5] **Farhat, C.**, CFD on Moving Grids: from theory to realistic flutter, maneuvering and multidisciplinary optimization, *International Journal of Computational Fluid Dynamics*, Vol 19 No 8, 2005
- [6] **Gordnier E. R., Fithen R.**, Coupling of a Nonlinear Finite Element Solver with a Navier-Stokes Solver, *Computers and Structures*, 2003, Vol.81, Iss.2; p.75-89
- [7] **Lohner, R.; Cebral, J.; Chi Yang; Baum, J.D.; Mestreau, E.; Charman, C.; Pelessone, D.;** Large-scale Fluid-structure Interaction Simulations, *Computing in Science and Engineering*, 2004, Vol.6, Iss.3 p.27-37
- [8] **Massjung, R.**, Discrete Conservation and Coupling Strategies in Nonlinear Aeroelasticity, *Computer Methods in Applied Mechanics and Engineering*, 2006, Vol.196, Iss.1-3; p.91
- [9] **Newmann, J. C., et al.**, Efficient Nonlinear Static Aeroelastic Wing Analysis, *Computers and Fluids*, 1999, Vol.28, Iss.4-5; p.615-628
- [10] **Suleman, A., Relvas, A.**, Fluid Structure Modeling of Nonlinear Aeroelastic Structures Using The Finite Element Corotational Theory, *Journal of Fluids and Structures*, 2006, Vol.22, Iss.1; p.59-75
- [11] **Liu, F., Tsai, H. M., Cai, J.**, Static Aeroelastic Computation with a Coupled CFD and CSD Method, *Journal Of Aircraft*, 1993
- [12] **Guruswamy, G., Garcia, C. J.**, Static Aeroelastic Characteristics of an Advanced Wing with a Control Surface Using Navier-Stokes Equations, AIAA-1999-796 *Aerospace Sciences Meeting and Exhibit*, 37th, Reno, NV, Jan. 11-14, 1999

- [13] **Relvas, A., Suleman, A.**, Aeroelasticity of Nonlinear Structures Using the Corotational Method, *Journal of Aircraft*, 2006, vol.43 no.3
- [14] **Newmann, J. C., Newman P. A., et. al.**, Efficient Nonlinear Static Aeroelastic Wing Analysis, *Computers and Fluids*, 1999, Volume 28, Issues 4-5; p.615
- [15] **Karpel, M., Yaniv, S., Livshits, S. D.**, Integrated Solution for Computational Static Aeroelastic Problems, *Symposium on Multidisciplinary Analysis and Optimization*, 6th, Bellevue, WA, Sept. 4-6, 1996, Technical Papers. Pt. 1
- [16] **Schuster, D., Vadyak, E., Atta, E.**, Static Aeroelastic Analysis of Fighter Aircraft Using a Three-Dimensional Navier-Stokes Algorithm, *Journal of Aircraft*, 1990, vol.27 no.9 (820-825)
- [17] **Liu, F., Cai, J., Tsai, H. M.**, Static Aero-elastic Computation with a Coupled CFD and CSD Method, *AIAA-2001-717 Aerospace Sciences Meeting and Exhibit*, 39th, Reno, NV, Jan. 8-11, 2001
- [18] **Guruswamy, G. P., Byun, C.**, Static Aeroelasticity Computations For Flexible Wing-Body Control Configurations, AIAA, NASA, and ISSMO, *Symposium on Multidisciplinary Analysis and Optimization*, 6th, Bellevue, WA, Sept. 4-6, 1996, Technical Papers. Pt. 1 (A96-38701 10-31), Reston, VA, American Institute of Aeronautics and Astronautics, 1996, p. 744-754
- [19] **Guruswamy, G. P., Kapania, R., Macmurdy, D.**, Static Aeroelastic Analysis of Wings Using Euler/Navier-Stokes Equations Coupled With Improved Wing-Box Finite Element Structures, *AIAA-1994-1587 IN:AIAA/ASME/ASCE/AHS/ASC Structures, Structural Dynamics, and Materials Conference*, 35th, Hilton Head, SC, Apr 18-20, 1994, Technical Papers. Pt. 4 (A94-23876 06-39), Washington, DC, American Institute of Aeronautics and Astronautics, 1994, p. 2146-2158
- [20] **Kamakoti, R., Lian, Y., et.al.**, Computational Aeroelasticity Using a Pressure-Based Solver, *AIAA Journal*, 2002, *40th AIAA Aerospace Sciences Meeting and Exhibit*, 14-17 January 2002 / Reno, Nevada
- [21] **Yates, E. C., Jr.**, AGARD Standard Aeroelastic Configuration for Dynamic Response I. AGARD 445.6, 1988, **AGARD REPORT No.765**
- [22] **Marjorie E. Munrb, Ken12etb J. R. Munning, Thomas H. Hallstag und John T, Rogers**, Transonic Pressure Measurements and Comparison of Theory to Experiment for an Arrow-Wing Configuration, 1976, **NASA CR-2610**
- [23] **Maynard C. Sandford, David A. Seidel, and Clinton V. Eckstrom**, Steady Pressure Measurements on an Aeroelastic Research Wing, 1994, NASA-IM-I09046
- [24] **Lieu,T., Farhat, C.**, Adaptation of POD-based Aeroelastic ROMs for Varying Mach Number and Angle of Attack: Application to a Complete F-16 Configuration,2005, *U.S. Air Force T&E Days*, 6 - 8 December 2005, Nashville, Tennessee

- [25] **Arora, J.S.**, *Introduction to optimum design*, Elsevier Academic Press, 2004
- [26] **Back, T., Hoffmeister, F. and Schwefel, H., P.**, A survey of evolution strategies, *Proceedings Fourth Int Conf. Genetic Algorithms*, ICGA, 1991.
- [27] **Barthelemy, J-F., Wrenn, G., Dovi, A. and Hall, L.**, Supersonic transport wing minimum design integrating aerodynamics and structures, *Journal of Aircraft*, 1994, 31:330-338
- [28] **Baysal, O. and Eleshaky, M. E.**, Aerodynamic design optimization using sensitivity analysis and computational fluid dynamics, *AIAA Journal*, 1992, 30 (3):718-725
- [29] **Bendsoe, M.**, *In Optimization of Structural Topology, Shape, and Material*, Berlin, Springer, 1995
- [30] **Bowman, K., Granddhi, R. and Eastep, F.**, Structural optimization of lifting surfaces with divergence and control reversal constraints, *Struct. Optim.*, 1989, 1:153-161
- [31] **Dovi, A.R. , Wrenn, G.A. , Barthelemy, J.F. , Coen, P.G. and Hall, L. E.**, Multidisciplinary Design Integration Methodology for a Supersonic Transport Aircraft, *Journal of Aircraft*, 1995, 32 (2):290-296
- [32] **Friedmann, P.**, Helicopter vibration reduction using structural optimization with aeroelastic/multidisciplinary constraints – a survey, *Journal of Aircraft* , 1991, 38:8-21
- [33] **Goldberg, D.**, *In Genetic Algorithms in Search. Optimization and Machine Learning*. Reading, M.A. Addison-Wesley, 1989
- [34] **Grierson, D. E. and Hajela, P.**, Emergent computing methods in engineering design-applications of genetic algorithms and neural networks. In *Nato asi series f: Computer and Systems Sciences*. 1996
- [35] **Guinta, A. and Sobiesczanski-Sobieski, J.**, Progress towards using sensitivity derivatives in a high-fidelity aeroelastic analysis of a supersonic transport. In *AIAA 98-4763. 7th AIAA/USAF/NASA/ISSMO Symposium on Multidisciplinary Analysis and Optimization*. St Louis, MO, pp 441-453, Sept 1998
- [36] **Jha, R. and Chattopadhyay, A.**, Multidisciplinary optimization of composite wings using refined structural and aeroelastic analysis methodologies. *Engineering Optimization*, 1999, 32:59-78
- [37] **Kirsch, U.**, *Structural Optimization: Fundamentals and Applications*. Berlin Springer, 1993
- [38] **Maute, K., Nikbay, M. and Farhat, C.**, Coupled analytical sensitivity analysis and optimization of three dimensional aeroelastic systems. *AIAA Journal*, 2001, 39 (11):2051-2061
- [39] **Maute, K., Nikbay, M. and Farhat, C.**, Coupled analytical sensitivity analysis for aeroelastic optimization. *AIAA 2000-4825, 8th AIAA/USAF/NASA/ISSMO Symposium on Multidisciplinary Analysis and Optimization*, September 6-8.2000/Long Beach. CA. AIAA. 2000

- [40] **Nikbay, M.**, Coupled sensitivity analysis by discrete-analytical direct and adjoint methods with applications to aeroelastic optimization and sonic boom minimization, PhD Thesis, University of Colorado at Boulder, 2002
- [41] **Schittkowski, K.**, NLPQL: A Fortran subroutine solving constrained nonlinear programming problems. *Annals of Operations Research*, 1985, 6:485-500
- [42] **Tzong, G., Baker, M., Vari, R.D. and Giesing, J.**, Aeroelastic loads and structural optimization of a high speed civil transport model. *5th AIAA/NASA/USAF/ISSMO Symp. On Multidisciplinary Analysis and Optimization*, Panama City Beach, FL. AIAA Paper No 94-4378. IAA 1994
- [43] **Kolonay, R. M.**, Unsteady Aeroelastic Optimization in the Transonic Regime, *AIAA, NASA, and ISSMO, Symposium on Multidisciplinary Analysis and Optimization*, 6th, Bellevue, WA, Sept. 4-6, 1996, Technical Papers. Pt. 1 (A96-38701 10-31), Reston, VA, American Institute of Aeronautics and Astronautics, 1996, p. 25-35
- [44] **DeLaurentis, D. A., Cesnik, C. E. S., Lee, J., et al.**, A new approach to Integrated Wing Design in Conceptual Synthesis and Optimization, *AIAA, NASA, and ISSMO, Symposium on Multidisciplinary Analysis and Optimization*, 6th, Bellevue, WA, Sept. 4-6, 1996, Technical Papers. Pt. 2 (A96-38701 10-31), Reston, VA, American Institute of Aeronautics and Astronautics, 1996, p. 1835-1843
- [45] **Battoo, R. S., Visser, J. A. P.**, Aeroelastic and Strength Optimization of Large Aircraft Wing with Wing Parameter Variation, *AIAA Journal*, 1998
- [46] **Ricci, S., Terraneo, M.**, Application of MDO techniques to the preliminary design of morphed aircraft, 11th AIAA/ISSMO Multidisciplinary Analysis and Optimization Conference 6 - 8 September 2006, Portsmouth, Virginia
- [47] **Martins, R., R., A., J., Alonso, J., J., Reuther, J.**, Complete Configuration Aero-Structural Optimization Using a Coupled Sensitivity Analysis Method, *9th AIAA/ISSMO Symposium on Multidisciplinary Analysis and Optimization*, 4-6 September 2002, Atlanta, Georgia
- [48] **Epstein, B., Peigin, S.**, Constrained Aerodynamic Optimization of Three-Dimensional Wings Driven by Navier–Stokes Computations, *AIAA Journal*, Vol. 43, No. 9, September 2005
- [49] **Guruswamy, G., Obayashi, S.**, Study on the Use of High-Fidelity Methods in Aeroelastic Optimization, *Journal of Aircraft*, Vol. 41, No. 3, May–June 2004
- [50] **Nikbay, M., Yanangönül, A., Öncü, L., Kocas, M.**, Multi-Objective and Gradient Based Structural Design Optimization of an Aircraft Wing, *Second International Conference on Multidisciplinary Design Optimization and Applications*, Gijon, Spain, 2008
- [51] **Haftka, R., T., Gürdal, Z.**, *Elements of Structural Optimization*, Kluwer Academic Publishers, 1992, Dordrecht

- [52] **Nikbay, M., Öncü, L., Aysan, A.**, A multidisciplinary code coupling approach for analysis and optimization of aeroelastic systems. *12th AIAA/ISSMO Multidisciplinary Analysis and Optimization Conference*, 10 – 12 Sep 2008, Victoria, British Columbia, Canada. AIAA, 2008
- [53] **Farhat, C.**, Special Course on Parallel Computing in CFD, 1995, **AGARD Report R-807**, pp. 8-1,8-79
- [54] **Farhat, C., Lesoinne, M., Maman, N.**, Mixed explicit/implicit time integration of coupled aeroelastic problems: Three field formulation, geometric conservation and distributed solution, *Int. Journal of Num. Meth. Fluids*, 1995, 21:807-835
- [55] **Farhat, C., Degand, C., Koobus, B., et al.**, Torsional springs for two-dimensional dynamic unstructured fluid meshes, *Comp. Meth. Appl. Mech. Eng.*, 163:231-245, 1998
- [56] **Maute, K., Nikbay, M., Farhat, C.**, Coupled analytical sensitivity analysis and optimization of three-dimensional nonlinear aeroelastic systems, *AIAA Journal*, 39 (11):2051-2061, 2001
- [57] **Farhat, C., Lesoinne, M.**, Two efficient staggered procedures for the serial and parallel solution of three-dimensional nonlinear transient aeroelastic problems, *Comp. Meth. Appl. Mech. Eng.*, 182:499-515, 2000
- [58] **Maman, N., Farhat, C.**, Matching fluid and structure meshes for aeroelastic computations: A parallel approach, *Comp. Struct.*, 54:779-785, 1995
- [59] **Weaver, W., Johnston, P. R.**, *Finite Elements For Structural Analysis*, Prentice-Hall Inc, 1984
- [60] **Yosibash, Z., Kirby, R. M., Myers, M., Szabo, B. and Karniadakis, G.**, High-order finite elements for fluid-structure interaction problems, *44th AIAA/ASME/ASCE/AHS Structures, Structural Dynamics and Materials Conference*, 7-10 April, Norfolk, Virginia, 2003
- [61] **Pham, L., Farhat, C.**, *TOP/DOMDEC User's Manual*, 2002

APPENDICES

APPENDIX A.1 : Geometric and Structural Model of the Reference Wing

APPENDIX B.1 : Structural Validation and Steady-State Aeroelastic
Analysis Results

APPENDIX A.1

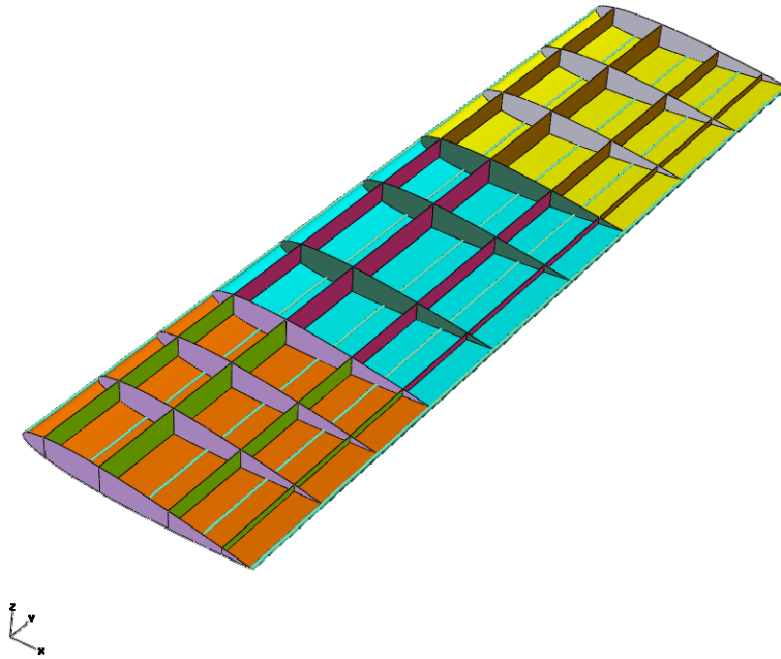


Figure A.1 : The optimization variables shown by colour groups

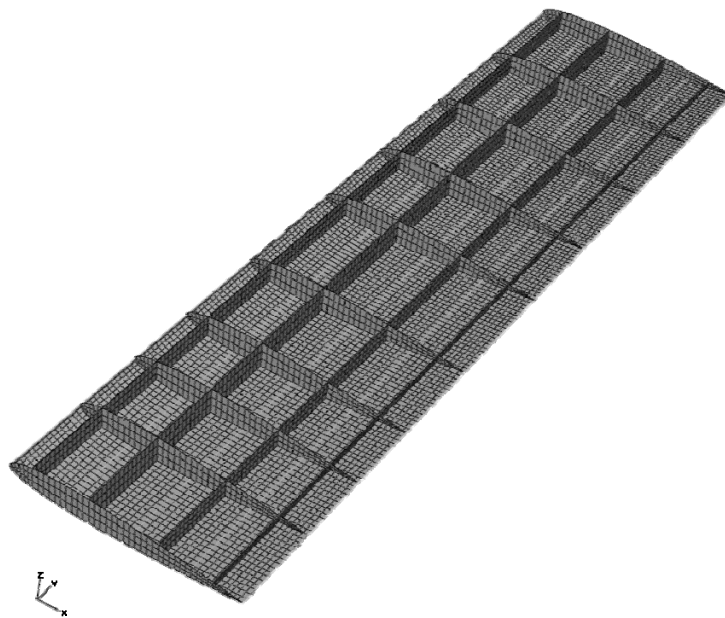


Figure A.2 : Quad dominated structural mesh of the wing

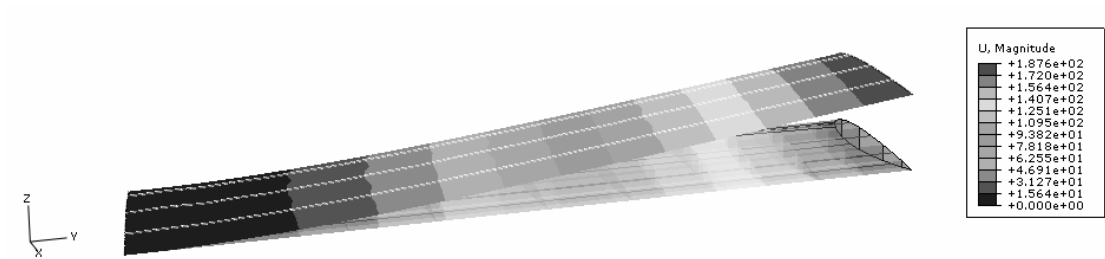


Figure A.3 : Displacement field of reference wing under static load (mm)

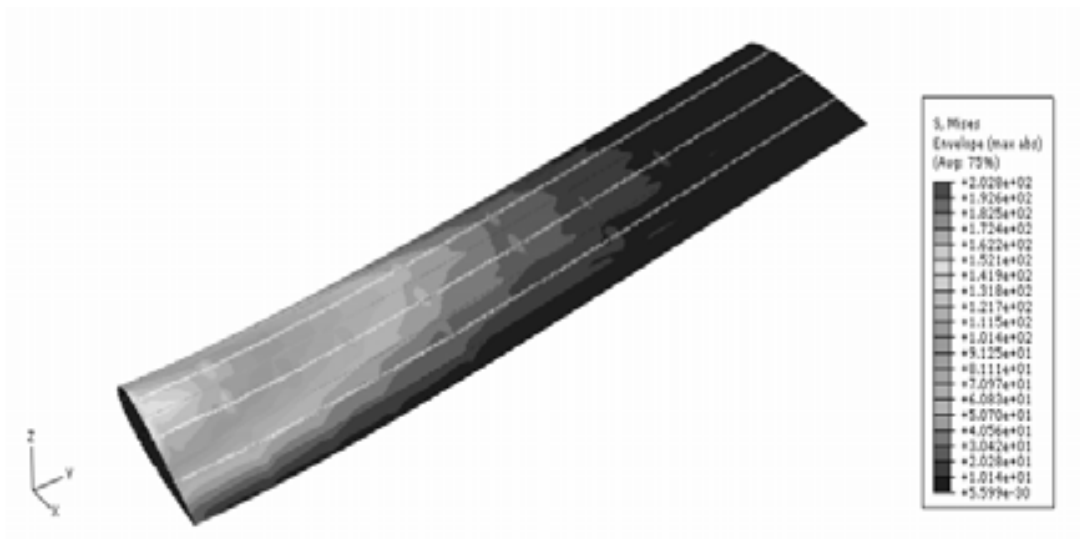


Figure A.4 : Stress field of reference wing under static load (MPa)

APPENDIX B.1

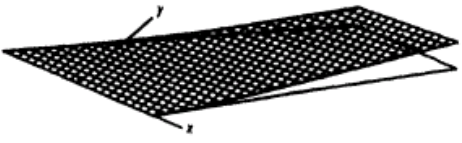
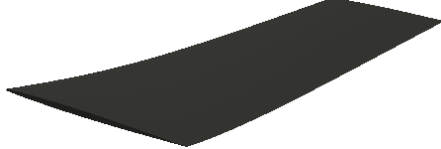
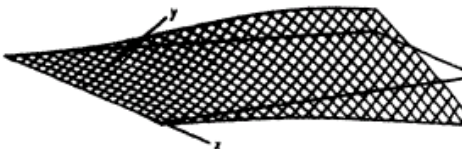
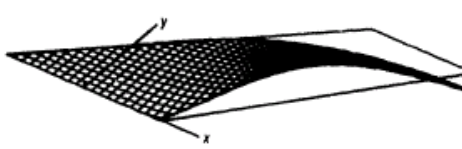
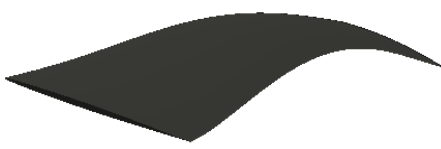
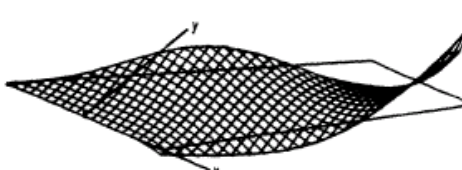
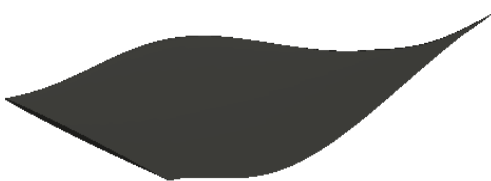
Experimental Data [21]	Present Study
 <p data-bbox="503 598 690 640">1st Bending Mode</p>	 <p data-bbox="974 609 1266 640">1st Bending Mode (9.61 Hz)</p>
 <p data-bbox="503 882 690 913">1st Torsion mode</p>	 <p data-bbox="974 882 1266 913">1st Torsion mode (37.33 Hz)</p>
 <p data-bbox="454 1123 738 1155">1st Bending/Torsion mode</p>	 <p data-bbox="925 1123 1323 1155">1st Bending/Torsion mode (55.94 Hz)</p>
 <p data-bbox="454 1417 738 1449">2nd Bending/Torsion Mode</p>	 <p data-bbox="917 1417 1331 1449">2nd Bending/Torsion Mode (104.12 Hz)</p>

Figure B.1: Computed modal shapes compared to experimental data

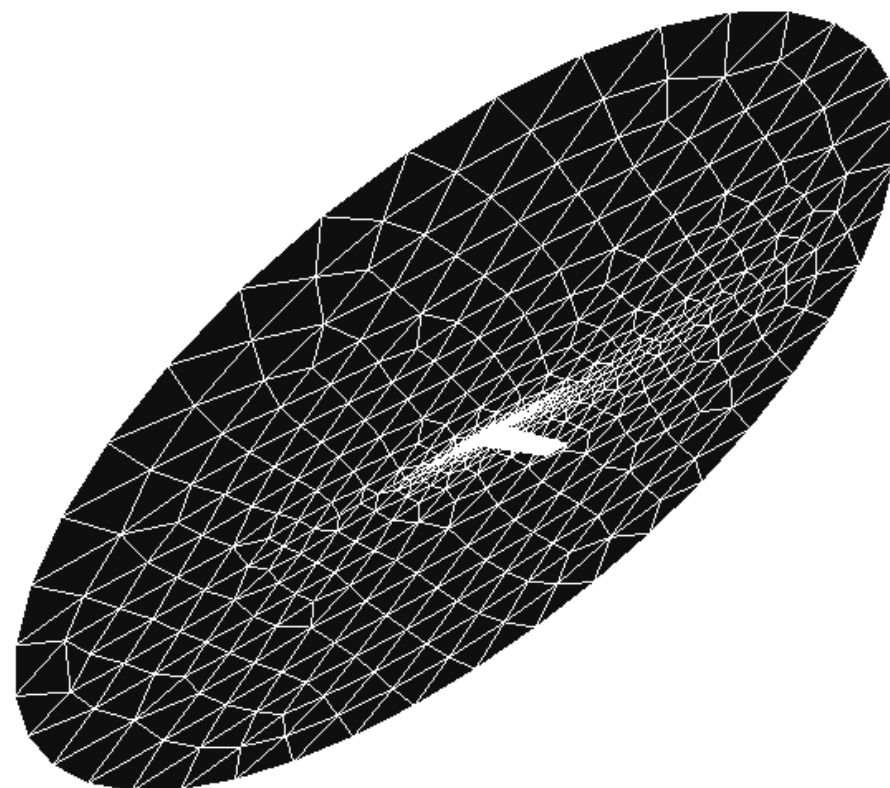


Figure B.2: Coarse CFD grid with 403321 tetras

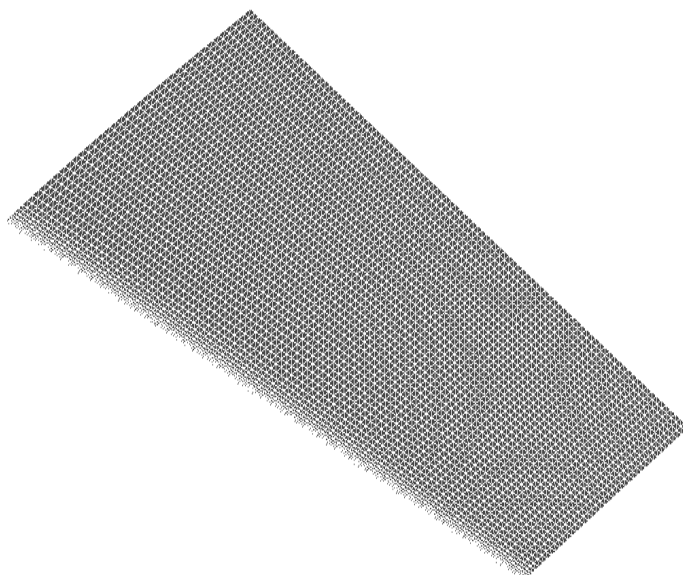


Figure B.3: Close-up to the wet surface of the wing

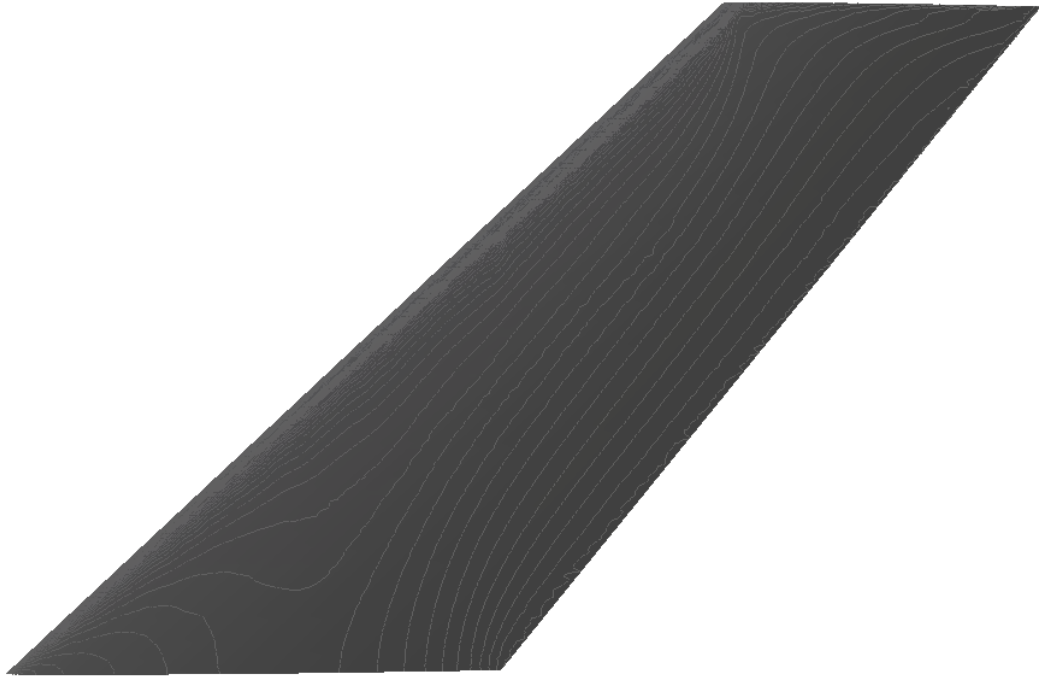


Figure B.4: Pressure contours for the upper surface of rigid wing, present study

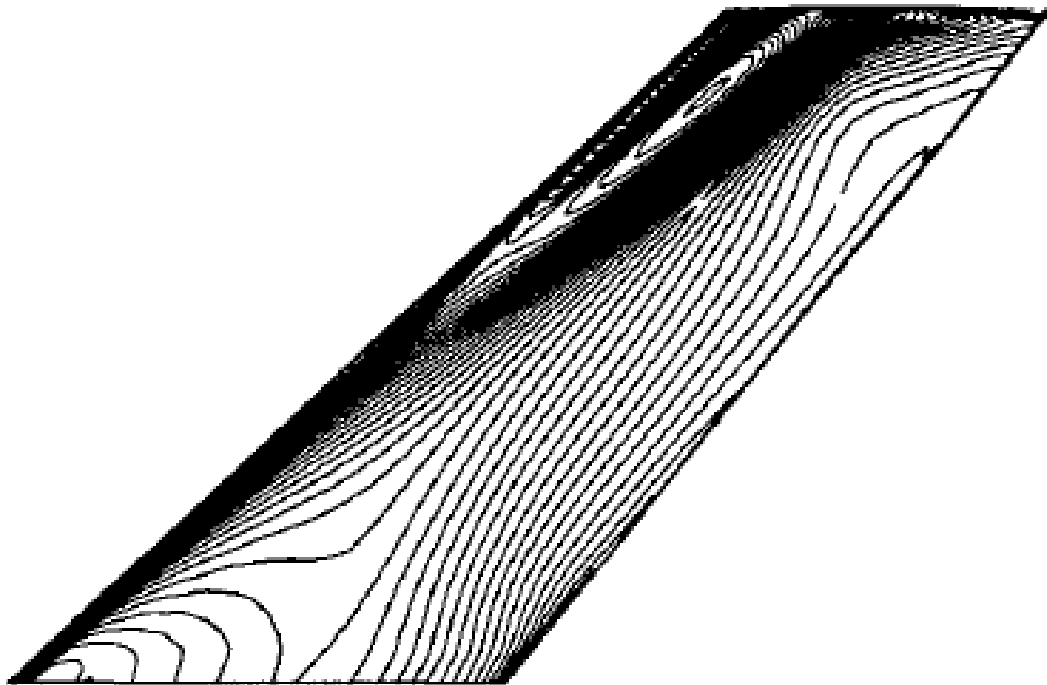


Figure B.5: Pressure contours for the upper surface of the rigid wing, Liu [11]

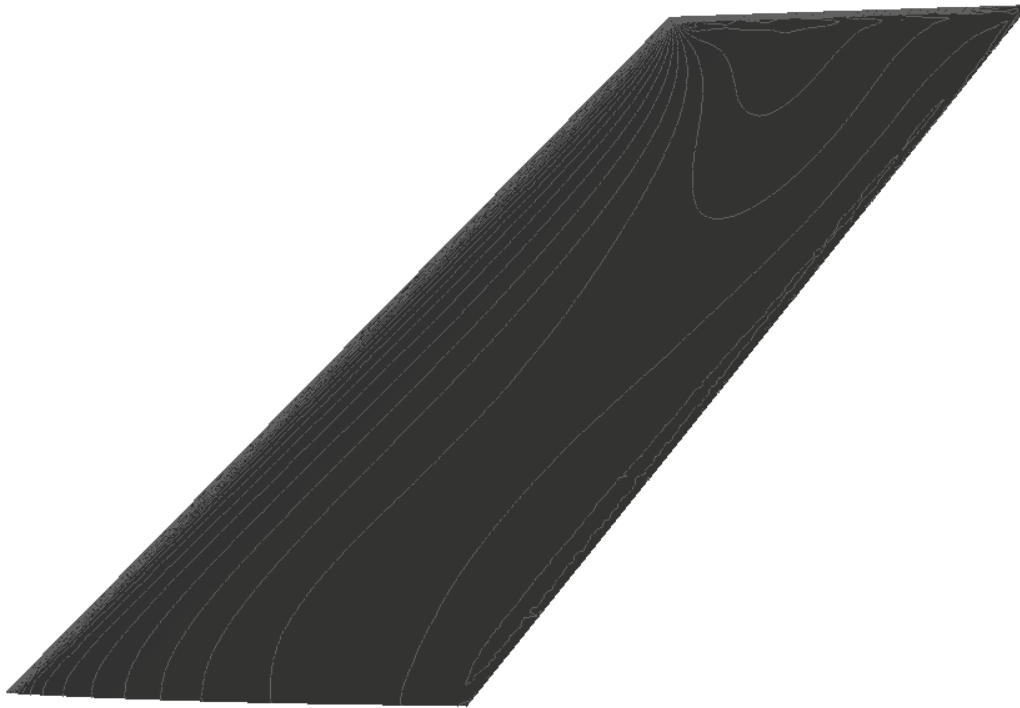


Figure B.6: Pressure contours for the lower surface of rigid wing, present study

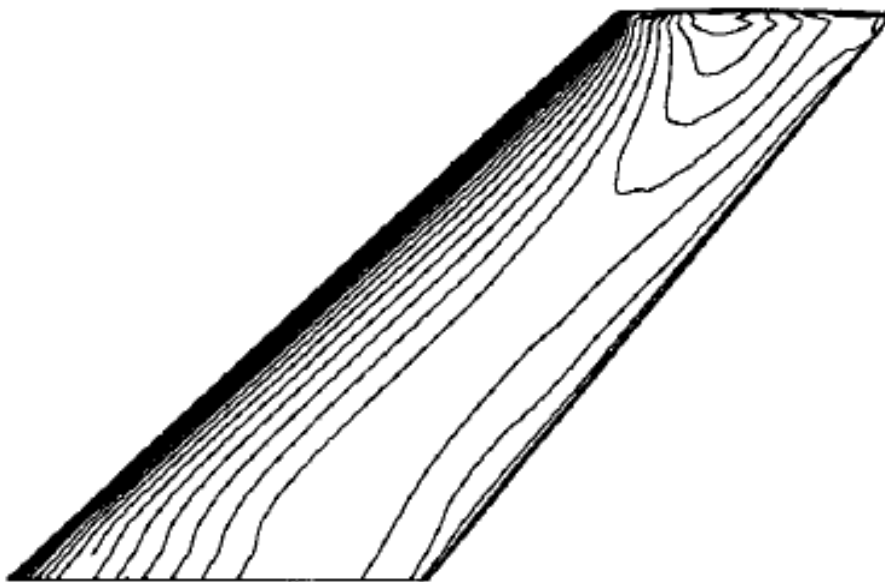


Figure B.7: Pressure contours for the upper surface of rigid wing, Liu [11]

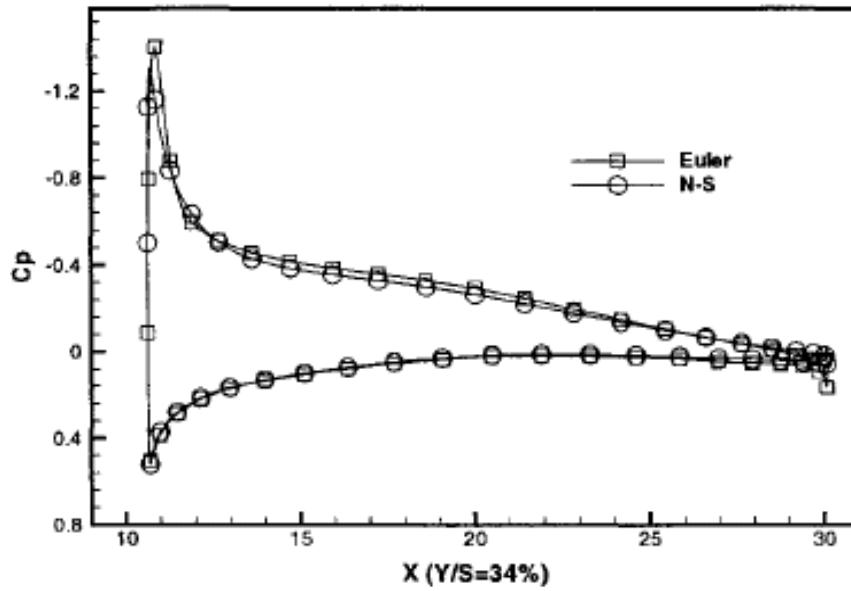


Figure B.8: Pressure coefficients for the elastic wing at 34% span, Liu [11]

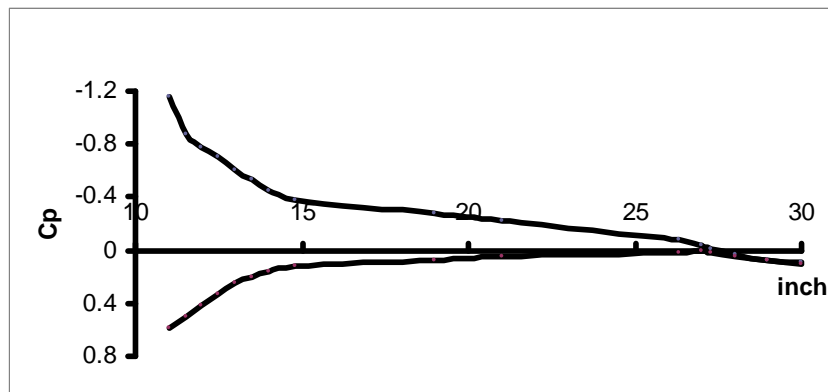


Figure B.9: Pressure coefficients for the elastic wing at 34% span, present study

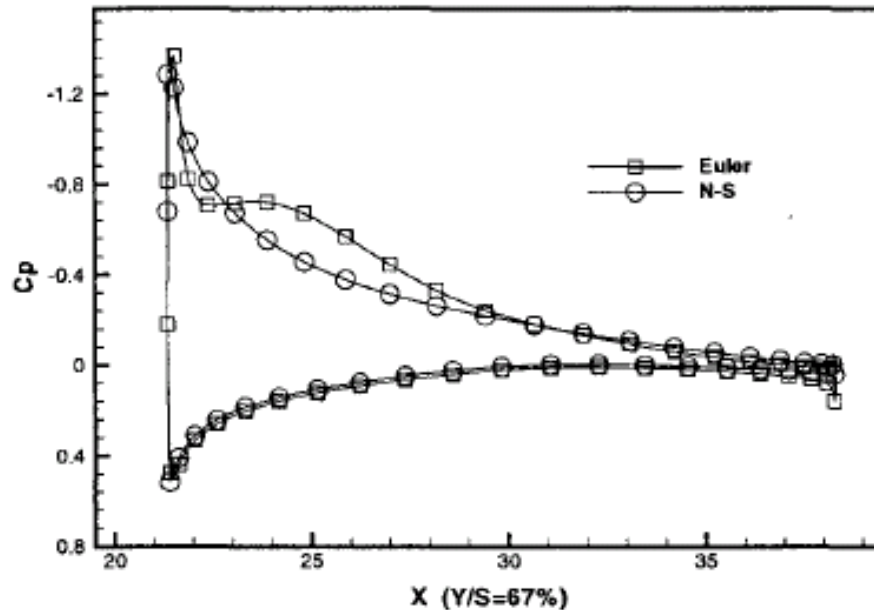


Figure B.10: Pressure coefficients for the elastic wing at 67% span, Liu [11]

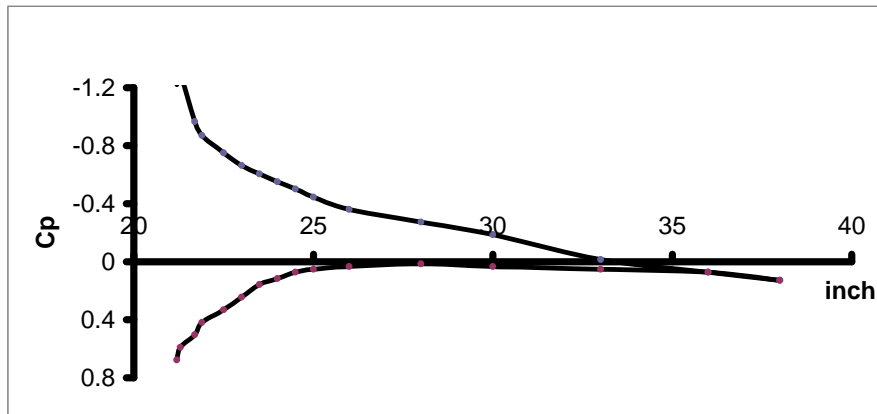


Figure B.11: Pressure coefficients for the elastic wing at 67% span, present study

CURRICULUM VITAE



Candidate's full name: Arda YANANGÖNÜL

Place and date of birth: Istanbul / 13.02.1982

Permanent Address: 2. Orta Sok. Sedir Apt. No: 11/13
Göztepe / Kadıköy / İstanbul

Universities and Colleges attended:

Istanbul Technical University	2006
Kadıköy Anadolu Lisesi	2001

Publications:

Nikbay, M., **Yanangönül, A.**, Öncü, L., Koçaş, M., Multi-Objective and Gradient Based Structural Design Optimization of an Aircraft Wing, *Second International Conference on Multidisciplinary Design Optimization and Applications*, Gijon, Spain, 2008

Nikbay, M., **Yanangönül, A.**, Öncü, L., Bir Uçak Kanadının Çok Amaçlı Genetik Algoritmalar ile Yapısal Optimizasyonu, *Kayseri VII. Havacılık Sempozyumu*, 2008

Öncü, L., **Yanangönül, A.**, Nikbay, M., Uçak-Uzay Yapılarının Statik Aeroelastik Kriter ile Çok Disiplinli Tasarım Optimizasyonu, *2. Ulusal Havacılık ve Uzay Konferansı*, İstanbul, İTÜ, 2008